

Majorana Tensor Decomposition: A unifying framework for decompositions of fermionic Hamiltonians to Linear Combination of Unitaries

Ignacio Loaiza^{1,2} and Artur F. Izmaylov^{1,2}

¹ University of Toronto, Department of Chemistry, Chemical Physics Theory Group, Toronto, ON, Canada

² University of Toronto Scarborough, Department of Physical and Environmental Sciences, Toronto, ON, Canada

(Dated: July 12, 2024)

Linear combination of unitaries (LCU) decompositions have appeared as one of the main tools for encoding operators on quantum computers, allowing efficient implementations of arbitrary operators. In particular, LCU approaches present a way of encoding information from the electronic structure Hamiltonian into a quantum circuit. Over the past years, many different decomposition techniques have appeared for the electronic structure Hamiltonian. Here we present the Majorana Tensor Decomposition (MTD), a framework that unifies existing LCUs and offers novel decomposition methods by using popular low-rank tensor factorizations.

I. INTRODUCTION

Quantum chemistry has appeared as one of the main contenders in the race for quantum supremacy. This problem consists in finding eigenvalues of the electronic structure Hamiltonian

$$\hat{H} = \sum_{ij}^N h_{ij} \hat{F}_j^i + \sum_{ijkl}^N g_{ijkl} \hat{F}_j^i \hat{F}_l^k, \quad (1)$$

where $\{i, j, k, l\}$ are spacial orbitals, h_{ij} and g_{ijkl} are one- and two-electron integrals¹, N is the number of spacial one-electron orbitals, and $\hat{F}_j^i \equiv \sum_{\sigma} \hat{a}_{i\sigma}^{\dagger} \hat{a}_{j\sigma}$ are spacial excitation operators, with $\sigma \in \{\alpha, \beta\}$ spin-z projections.

Efficiently finding eigenvalues of the electronic structure Hamiltonian can be achieved on a quantum computer through algorithms such as quantum phase estimation (QPE) and its variants [1–9]. These algorithms require the implementation of functions of the Hamiltonian, such as the time evolution operator $e^{-i\hat{H}t}$, within the quantum circuit to incorporate information from \hat{H} . Generally, there are two approaches for encoding \hat{H} on a quan-

tum circuit: Trotter product formulas [10–12] and LCU-based encodings. Product formula approaches involve decomposing \hat{H} into a sum of fast-forwardable fragments to implement the time-evolution operator. Despite its advantages and low qubit costs, this family of approaches does not provide the optimal $\sim \mathcal{O}(t)$ time scaling [13–15]. On the other hand, LCU-based encodings construct an \hat{H} oracle circuit and enable the implementation of an arbitrary polynomial of \hat{H} [16–18]. The LCU encoding also gives rise to the qubitization approach implementing a walk operator [17, 19, 20] denoted as $\hat{\mathcal{W}}$, which has eigenvalues $e^{\pm i \text{arccos}(E_n/\lambda)}$, where E_n are the eigenvalues of \hat{H} (see Fig. 1) and $\lambda = \sum_k |u_k|$ is a 1-norm of a coefficient vector for an LCU decomposition of H

$$\hat{H} = \sum_{k=1}^K u_k \hat{U}_k. \quad (2)$$

Here, \hat{U}_k are unitary operators, u_k are complex coefficients, and K is the total number of unitaries. By estimating the phase of the walker operator, the eigen-values of \hat{H} can be extracted from $\text{arccos}(E_n/\lambda)$. The accuracy associated with the energy estimation is upper-bounded by $\epsilon \leq \lambda \epsilon_W$, where ϵ_W is the walker operator phase estimation accuracy. Consequently, employing an optimal phase estimation algorithm with Heisenberg scaling $\mathcal{O}(1/\epsilon_W)$ [5, 9], the algorithm's cost to achieve a target energy accuracy of ϵ would require $\tilde{\mathcal{O}}(\lambda/\epsilon)$ calls to the walker operator. It is evident that the cost of the LCU-based energy estimation method depends on both the 1-norm λ and the implementation cost of the walker operator.

In this work, we consider lowering the circuit cost of the LCU-based Hamiltonian encoding [21] by optimizing the choice of unitary operators. The circuit cost of LCU decomposition is proportional to its 1-norm λ . By employ-

¹ Representing the Hamiltonian using only excitation operators is usually referred to as chemists' notation. This entails a modification to the one-electron tensor with respect to physicists' notation, which uses normal-ordered operators of the form $\hat{a}_p^{\dagger} \hat{a}_q^{\dagger} \hat{a}_r \hat{a}_s$. Our notation is related to the electronic integrals by $g_{ijkl} = \frac{1}{2} \int \int d\vec{r}_1 d\vec{r}_2 \frac{\phi_i^*(\vec{r}_1) \phi_j(\vec{r}_1) \phi_k^*(\vec{r}_2) \phi_l(\vec{r}_2)}{|\vec{r}_1 - \vec{r}_2|}$ and $h_{ij} = - \sum_k g_{ikkj} + \int d\vec{r} \phi_i^*(\vec{r}) \left(-\frac{\nabla^2}{2} - \sum_n \frac{Z_n}{|\vec{r} - \vec{R}_n|} \right) \phi_j(\vec{r})$, with $\phi_i(\vec{r})$ the one-particle electronic basis functions, and Z_n/\vec{R}_n the charge/position of nucleus n .

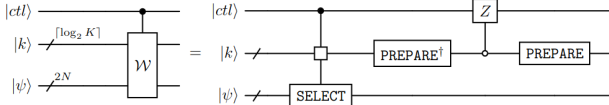


Figure 1. LCU-based implementation of walk operator with eigenvalues $e^{\pm i \arccos \frac{\hat{H}}{\lambda}}$, for $\lambda = \sum_k |c_k|$ the 1-norm of the LCU. Note the Z gate is applied conditioned on the state of all qubits in register k to be zero.

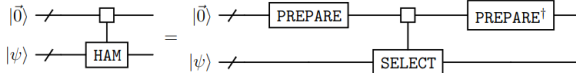


Figure 2. LCU Hamiltonian oracle implementation by block encoding with output $|0\rangle_a \otimes \frac{\hat{H}}{\lambda} |\psi\rangle + |\text{remainder}\rangle$. PREPARE $|0\rangle_a = \sum_k \sqrt{\frac{w_k}{\lambda}} |k\rangle_a$ and SELECT $= \sum_k |k\rangle \langle k|_a \otimes \hat{U}_k$ for the LCU shown in Eq. (2) and $|k\rangle_a$ the k -th state of the ancilla register, requiring $\lceil \log_2 M \rceil$ ancilla qubits, where M is the total number of unitaries in the LCU.

ing the LCU decomposition, we can construct a Hamiltonian oracle, which corresponds to a circuit that encodes the action of \hat{H}/λ on a quantum register [21, 22], as illustrated in Fig. 2. The spectral range $\Delta E \equiv E_{\max} - E_{\min}$, where $E_{\max(\min)}$ represents the maximum (minimum) eigenvalue of \hat{H} , provides a lower bound for the 1-norm, given by $\lambda \geq \Delta E/2$ [23]. Based on this consideration, it becomes evident that the eigenvalues of \hat{H}/λ after a constant shift will fall within the range of $[-1, 1]^2$. Having the Hamiltonian's spectrum within this range is necessary to ensure that the block encoding defines a unitary transformation in the quantum register plus ancilla space. Numerous LCU decompositions have been proposed for the electronic structure Hamiltonian [20, 23–25]. In this work, we present a unified framework for expressing the electronic structure Hamiltonian as an LCU. In addition, by working using polynomials of Majorana operators, we expect these decompositions to be applicable to other kind of Hamiltonians, such as the second-quantized form of a vibrational Hamiltonian [26]. This unified framework enables us to establish connections and to generalize existing decomposition methods.

To provide an appropriate context for comparison of

different LCUs, let us consider the main contributions to their quantum resource cost. The LCU-based Hamiltonian oracle shown in Fig. 2 comprises two primary components: the PREPARE circuit, which transforms the ancilla state $|0\rangle_a$ into a linear superposition with the LCU coefficients, and the SELECT circuit, which applies the LCU unitaries in a controlled manner. In general, it is possible to move operations from SELECT into PREPARE and vice-versa, and for a given LCU there might be several different associated oracles that realize the block-encoding. The unitaries in SELECT correspond to multiplexed operators [27, 28], and their quantum gate cost depends on that of the associated unitaries \hat{U}_k and a unary iteration over k indices [29]. The unary iteration is analogous to a for-loop over indices k conditionally applying \hat{U}_k , and it can be efficiently incorporated by using a binary tree algorithm [30]. This incurs an overhead scaling of $4(K-1)$ T-gates and $\lceil \log_2(K) \rceil - 1$ additional ancilla qubits. However, specific structures within the LCU decomposition can enable more efficient SELECT circuits. We will explore this aspect further after introducing the different LCU decomposition techniques.

The rest of this paper is organized as follows. Section II presents the unified Majorana tensor decomposition (MTD) framework for LCU decompositions and a new LCU decomposition. Then a list of recently proposed LCU decompositions expressed as MTDs is given in Sec. III. Finally, benchmarks for small systems and concluding remarks are offered in Sec. IV.

II. MAJORANA TENSOR DECOMPOSITION FRAMEWORK

We will use the Majorana operators formalism because it provides a convenient bridge between fermionic and qubit operators. Majorana operators are defined as

$$\hat{\gamma}_{j\sigma,0} \equiv \hat{a}_{j\sigma} + \hat{a}_{j\sigma}^\dagger \quad (3)$$

$$\hat{\gamma}_{j\sigma,1} \equiv i \left(\hat{a}_{j\sigma}^\dagger - \hat{a}_{j\sigma} \right), \quad (4)$$

with the algebraic relations

$$\{ \hat{\gamma}_p, \hat{\gamma}_q \} = 2\delta_{pq}\hat{1} \quad (5)$$

$$\hat{\gamma}_p^\dagger = \hat{\gamma}_p \quad (6)$$

$$\hat{\gamma}_p^2 = \hat{1}, \quad (7)$$

where we used complex indices p and q containing sub-indices $\{j\sigma, m\}$: $m \in \{0, 1\}$, j is a spacial orbital index, and $\sigma \in \{\alpha, \beta\}$ is the spin-z projection. The electronic structure Hamiltonian for closed-shell systems can

² A constant shift should also be considered to center the spectrum around 0. However, the discussion of such constant shifts is omitted as they can be easily added due to their commutativity with all operators.

be written in the Majorana representation as [23, 31]

$$\begin{aligned}\hat{H} &= \left(\sum_i h_{ii} + \sum_{ij} g_{iijj} \right) \hat{1} \\ &+ \frac{i}{2} \sum_{\sigma} \sum_{ij} \left(h_{ij} + 2 \sum_k g_{ijkk} \right) \hat{\gamma}_{i\sigma,0} \hat{\gamma}_{j\sigma,1} \\ &- \frac{1}{4} \sum_{\sigma\tau} \sum_{ijkl} g_{ijkl} \hat{\gamma}_{i\sigma,0} \hat{\gamma}_{j\sigma,1} \hat{\gamma}_{k\tau,0} \hat{\gamma}_{l\tau,1}.\end{aligned}\quad (8)$$

$$\equiv \hat{H}_0 + \hat{H}_1 + \hat{H}_2,\quad (9)$$

where we have respectively defined the zero-, two-, and four-Majorana components \hat{H}_0 , \hat{H}_1 , and \hat{H}_2 .

Since no terms with more than four Majorana operators appear in \hat{H} , a general MTD representation of the Hamiltonian can be written as

$$\hat{H} = \sum_{\substack{w_1, \dots, w_L \\ m_1, \dots, m_L}} \Omega_{\vec{w}, \vec{m}} \prod_{\nu=1}^L \hat{V}_{\vec{m}}^{(\nu)\dagger} \hat{p}_{\vec{w}}^{(\nu)} \hat{V}_{\vec{m}}^{(\nu)},\quad (10)$$

where $\Omega_{\vec{w}, \vec{m}}$ is a tensor with possibly complex coefficients, $\hat{p}_{\vec{w}}^{(\nu)}$ is a unitary operator expressed as a polynomial of Majorana operators of degree ≤ 4 with a minimal number of terms, $\hat{V}_{\vec{m}}^{(\nu)} \equiv e^{\sum_{p>q} \theta_{pq}^{(\vec{m}, \nu)} \hat{\gamma}_p \hat{\gamma}_q} \in \text{Spin}(4N)$ are unitary rotations that conserve the degree of $\hat{p}_{\vec{w}}^{(\nu)}$. For all decompositions shown in this work only spacial orbital rotations are used, which form a subgroup of $\text{Spin}(4N)$

$$\hat{U}_{\vec{\theta}} \equiv \exp \left[\sum_{i>j} \theta_{ij} (\hat{F}_j^i - \hat{F}_i^j) \right] \in \text{Spin}(N)\quad (11)$$

$$= \exp \left[\sum_{i>j} \frac{\theta_{ij}}{2} \sum_{\sigma} (\hat{\gamma}_{i\sigma,0} \hat{\gamma}_{j\sigma,0} + \hat{\gamma}_{i\sigma,1} \hat{\gamma}_{j\sigma,1}) \right].\quad (12)$$

For example, in the linear case $\hat{p}_1^{\nu} = \gamma_{1\sigma,x}$, where $x = \{0, 1\}$, all other linear in Majorana unitary operators can be obtained by conjugating with $\hat{U}_{\vec{\theta}}$ these two polynomials. For higher polynomial degrees, there is a still relatively low number of distinct $\hat{p}_{\vec{w}}^{(\nu)}$'s that give non-overlapping sets of unitary operators upon $\hat{U}_{\vec{\theta}}$ conjugation. We constrain the product $\prod_{\nu=1}^L \hat{p}_{\vec{w}}^{(\nu)}$ to yield a Majorana polynomial of degree ≤ 4 for all w_1, \dots, w_L appearing in the sum, which restricts $L \leq 4$.

Note that even though \hat{H} could be in principle decomposed with unitaries that are Majorana polynomials of degree > 4 , these contributions would have to cancel to

recover \hat{H} . Since there is an exponential number of Majorana polynomials with degree larger than 4, keeping track of these operators and enforcing their cancellation is a computationally daunting task. By enforcing conservation of the Majorana polynomial degree and starting with polynomials of degree ≤ 4 , we do not have to consider an exponentially large space, making the space of unitaries for the LCU more computationally tractable.

A. MTD- L^4 decomposition

The idea behind the MTD- L^4 decomposition is representing unitaries as products of four unitaries that are first degree polynomials of Majoranas, thus having $L = 4$. A way of writing this decomposition that conserves the spin-symmetry in Eq. (1) is

$$\hat{H}_2 = \sum_{\vec{m}} \Omega_{\vec{m}} \sum_{\sigma\tau} \hat{q}_{\vec{m}\sigma,0}^{(1)} \hat{q}_{\vec{m}\sigma,1}^{(2)} \hat{q}_{\vec{m}\tau,0}^{(3)} \hat{q}_{\vec{m}\tau,1}^{(4)},\quad (13)$$

where

$$\hat{q}_{\vec{m}\sigma,x}^{(\nu)} = \hat{U}_{\vec{m}}^{(\nu)\dagger} \hat{\gamma}_{1\sigma,x} \hat{U}_{\vec{m}}^{(\nu)}\quad (14)$$

for $x = 0, 1$. Here, we skip the \hat{H}_1 part since there is a known optimal treatment of this part, and it will be discussed with other fermionic LCU decomposition techniques in Sec. III B. Note that real orbital rotations \hat{U} 's [Eq. (12)] do not introduce Majoranas with different x or σ indices:

$$\hat{U}^{\dagger} \hat{\gamma}_{i\sigma,x} \hat{U} = \sum_j U_{ij} \hat{\gamma}_{j\sigma,x}.\quad (15)$$

Thus, the MTD- L^4 decomposition expresses the four-Majorana tensor, with associated rank = 4, as a linear combination of outer products of four rank-1 vectors, with a trivial index $\vec{w} = 1$. Generally, the orbital rotations can be implemented as products of Givens rotations with $\mathcal{O}(N^2)$ operations for rotating N orbitals. However, the orbital rotations shown here only act on a single spacial orbital, thus, only $\mathcal{O}(N)$ operations are necessary to implement these \hat{U} 's using Givens rotations. The corresponding angles of the Givens rotations can be found once the coefficients in Eq. (15) have been specified; a detailed discussion of how to find these coefficients is shown in Sec. III A 2.

Next, we show different ways of obtaining the MTD- L^4 decomposition using common tensor decomposition techniques.

1. MPS-based MTD- L^4

Matrix product state (MPS) formalism [32] applied to 4-index tensor g_{pqrs} can be seen as iterative application of the singular value decomposition (SVD) (see Fig.(3)). The SVD of a matrix is

$$A_{uv} = \sum_{\alpha} U_{u\alpha} S_{\alpha} W_{v\alpha}. \quad (16)$$

Treating the g_{ijkl} tensor as a matrix with indices i and jk allows to start the decomposition as follows

$$g_{ijkl} = \sum_{u=1}^N U_{iu}^{(1)} S_u^{(1)} W_{jklu}^{(1)} \quad (17)$$

$$= \sum_{u=1}^N \sum_{v=1}^{N^2} S_u^{(1)} S_v^{(2)} U_{iu}^{(1)} U_{jv}^{(2,u)} W_{klv}^{(2)} \quad (18)$$

$$= \sum_{u,w=1}^N \sum_{v=1}^{N^2} S_u^{(1)} S_v^{(2)} S_w^{(3)} U_{iu}^{(1)} U_{jv}^{(2,u)} U_{kw}^{(3,v)} W_{lw}^{(3)}. \quad (19)$$

From this, we can write

$$\hat{H}_2 = \sum_{ijkl} \sum_{uvw} \Omega_{uvw} U_{iu}^{(1)} U_{jv}^{(2,u)} U_{kw}^{(3,v)} W_{lw}^{(3)} \sum_{\sigma\tau} \hat{\gamma}_{i\sigma,0} \hat{\gamma}_{j\sigma,1} \hat{\gamma}_{k\tau,0} \hat{\gamma}_{l\tau,1} \quad (20)$$

$$= \sum_{uvw} \Omega_{uvw} \sum_{\sigma\tau} \hat{q}_{u,\sigma}^{(1)} \hat{q}_{uv,\sigma}^{(2)} \hat{q}_{vw,\tau}^{(3)} \hat{q}_{w,\tau}^{(4)}, \quad (21)$$

where we use the notation for the rotated polynomials

$$\hat{q}_{u,\sigma}^{(1)} \equiv \sum_i U_{iu}^{(1)} \hat{\gamma}_{i\sigma,0} \equiv \hat{U}_{1,u}^{\dagger} \hat{\gamma}_{1\sigma,0} \hat{U}_{1,u} \quad (22)$$

$$\hat{q}_{uv,\sigma}^{(2)} \equiv \sum_j U_{jv}^{(2,u)} \hat{\gamma}_{j\sigma,1} \equiv \hat{U}_{2,uv}^{\dagger} \hat{\gamma}_{1\sigma,1} \hat{U}_{2,uv} \quad (23)$$

$$\hat{q}_{vw,\tau}^{(3)} \equiv \sum_k U_{kw}^{(3,v)} \hat{\gamma}_{k\tau,0} \equiv \hat{U}_{3,vw}^{\dagger} \hat{\gamma}_{1\tau,0} \hat{U}_{3,vw} \quad (24)$$

$$\hat{q}_{w,\tau}^{(4)} \equiv \sum_l W_{lw}^{(3)} \hat{\gamma}_{l\tau,1} \equiv \hat{U}_{4,w}^{\dagger} \hat{\gamma}_{1\tau,1} \hat{U}_{4,w} \quad (25)$$

and $\Omega_{uvw} \equiv S_u^{(1)} S_v^{(2)} S_w^{(3)}$. Since in this case the SVD yields real unitary matrices U and W , it follows that for all of these polynomials $\hat{q} = \sum_p c_p \hat{\gamma}_p$, $c_p \in \mathbb{R}$ and $\sum_p |c_p|^2 = 1$, thus proving that these are real orbital rotations $\in \text{Spin}(N)$. The iterative SVD procedure for the g_{ijkl} tensor can be done efficiently on a classical computer, producing all necessary quantities for obtaining the LCU and specifying the corresponding unitaries. We will refer to this decomposition as the MPS decomposition. Note that the MPS decomposition can be done also by first factorizing the middle index with N^2 components. This decomposition would be extremely similar to the double factorization (DF) factorization of the two-electron tensor, although with a different LCU representation of the Hamiltonian.

2. CP4-based MTD- L^4

Alternatively the g_{ijkl} tensor can be decomposed as a linear combination of outer products of rank-1 vectors based on the CP4 tensor decomposition[33–38]

$$g_{ijkl} = \sum_m \Omega_m v_i^{(1,m)} v_j^{(2,m)} v_k^{(3,m)} v_l^{(4,m)}, \quad (26)$$

where each $\vec{v}^{(n,m)}$ for $n = 1, 2, 3, 4$ is an N -dimensional normalized vector. The associated MPS representation would correspond to a linear combination of MPSs with bond dimension 1, and is shown in Fig.4. Note that the normalization can be done without loss of generality since all normalization constants can be absorbed in the Ω_m coefficient. Obtaining the CP4 decomposition of the g_{ijkl} tensor also defines an MTD- L^4 decomposition as shown in Eq. (13), with the polynomials

$$\hat{q}_{m,\sigma}^{(1)} \equiv \sum_i v_i^{(1,m)} \hat{\gamma}_{i\sigma,0} = \hat{U}_m^{(1)\dagger} \hat{\gamma}_{1\sigma,0} \hat{U}_m^{(1)} \quad (27)$$

$$\hat{q}_{m,\sigma}^{(2)} \equiv \sum_j v_j^{(2,m)} \hat{\gamma}_{j\sigma,1} = \hat{U}_m^{(2)\dagger} \hat{\gamma}_{1\sigma,1} \hat{U}_m^{(2)} \quad (28)$$

$$\hat{q}_{m,\tau}^{(3)} \equiv \sum_k v_k^{(3,m)} \hat{\gamma}_{k\tau,0} = \hat{U}_m^{(3)\dagger} \hat{\gamma}_{1\tau,0} \hat{U}_m^{(3)} \quad (29)$$

$$\hat{q}_{m,\tau}^{(4)} \equiv \sum_l v_l^{(4,m)} \hat{\gamma}_{l\tau,1} = \hat{U}_m^{(4)\dagger} \hat{\gamma}_{1\tau,1} \hat{U}_m^{(4)}, \quad (30)$$

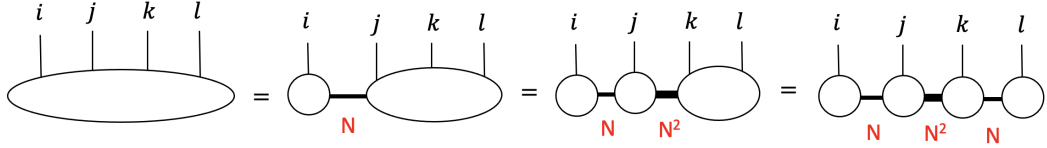


Figure 3. MPS diagram representation of iterative factorization of two-electron tensor with nested SVDs. Numbers in red show bond dimension for the matrices in the MPS.

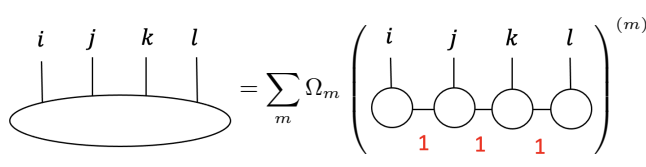


Figure 4. MPS representation of CP4 factorization.

which are implemented using $\text{Spin}(N)$ rotations as shown for the MPS LCU.

3. SVD-based MTD- L^4

There is yet another alternative scheme of iterative SVD for performing MTD- L^4 . This scheme groups indices differently than the MPS scheme,

$$g_{ijkl} = \sum_{\alpha_1=1}^N U_{i\alpha_1}^{(1)} S_{\alpha_1}^{(1)} V_{jkl}^{(1,\alpha_1)} \quad (31)$$

$$= \sum_{\alpha_1=1}^N U_{i\alpha_1}^{(1)} S_{\alpha_1}^{(1)} \sum_{\alpha_2=1}^N U_{j\alpha_2}^{(2,\alpha_1)} S_{\alpha_2}^{(2,\alpha_1)} V_{kl}^{(2,\alpha_1\alpha_2)} \quad (32)$$

$$= \sum_{\alpha_1=1}^N U_{i\alpha_1}^{(1)} S_{\alpha_1}^{(1)} \sum_{\alpha_2=1}^N U_{j\alpha_2}^{(2)} S_{\alpha_2}^{(2,\alpha_1)} \times \dots \dots \times \sum_{\alpha_3=1}^N U_{k\alpha_3}^{(3)} S_{\alpha_3}^{(3,\alpha_1\alpha_2)} V_l^{(3,\alpha_1\alpha_2\alpha_3)} \quad (33)$$

This decomposition gives rise to an MTD for which $\vec{m} \cong (\alpha_1, \alpha_2, \alpha_3)$ with N^3 elements. This MTD is then deter-

mined by

$$\hat{q}_{\alpha_1\alpha_2\alpha_3,\sigma}^{(1)} = \sum_i U_{i\alpha_1}^{(1)} \hat{\gamma}_{i\sigma,0} \quad (34)$$

$$\hat{q}_{\alpha_1\alpha_2\alpha_3,\sigma}^{(2)} = \sum_j U_{j\alpha_2}^{(2,\alpha_1)} \hat{\gamma}_{j\sigma,1} \quad (35)$$

$$\hat{q}_{\alpha_1\alpha_2\alpha_3,\tau}^{(3)} = \sum_k U_{k\alpha_3}^{(3,\alpha_1\alpha_2)} \hat{\gamma}_{k\tau,0} \quad (36)$$

$$\hat{q}_{\alpha_1\alpha_2\alpha_3,\tau}^{(4)} = \sum_l V_l^{(3,\alpha_1\alpha_2\alpha_3)} \hat{\gamma}_{l\tau,1} \quad (37)$$

$$\Omega_{\alpha_1\alpha_2\alpha_3} = S_{\alpha_1}^{(1)} S_{\alpha_2}^{(2,\alpha_1)} S_{\alpha_3}^{(3,\alpha_1\alpha_2)}. \quad (38)$$

Note that if we “flatten” the $N \times N \times N$ vector $(\alpha_1, \alpha_2, \alpha_3)$ into a one-dimensional array with N^3 elements, we recover an MTD which is identical to the MTD-CP4, the only difference being how the tensor was decomposed. We refer to this family of decompositions as MTD- L^4 . However, the additional structure in some of these decompositions (e.g., MPS) make it amenable to more efficient LCU oracles, as shown in the circuits in the Appendix A.

III. CURRENT LCUs AS MTDs

Here we show how current LCUs can be written as MTDs, these mappings are summarized in Table III B 4.

A. Qubit-based decompositions

1. Pauli product decompositions

Also known as the sparse LCU, the simplest LCU decomposition can be obtained by mapping the electronic structure Hamiltonian [Eq. (1)] into qubit operators through the use of some fermion-to-qubit mapping (e.g., Jordan-Wigner [39] or Bravyi-Kitaev [40–42]):

$$\hat{H} = \sum_q d_q \hat{P}_q, \quad (39)$$

where d_q are coefficients for the electronic structure Hamiltonian, and \hat{P}_q are products of Pauli operators over qubits, commonly referred to as Pauli products.

To see the correspondence between electron integrals in the fermionic Hamiltonian Eq. (1) and coefficients of Pauli products (d_q), it is convenient to write the fermionic Hamiltonian using the reflection operators $\hat{Q}_{kl\sigma} \equiv i\hat{\gamma}_{k\sigma,0}\hat{\gamma}_{l\sigma,1}$:

$$\hat{H} = \hat{H}_0 + \frac{1}{2} \sum_{ij} \tilde{h}_{ij} \sum_{\sigma} \hat{Q}_{ij\sigma} + \frac{1}{4} \sum_{ijkl} g_{ijkl} \sum_{\sigma\tau} \hat{Q}_{ij\sigma} \hat{Q}_{kl\tau}, \quad (40)$$

where we have defined $\tilde{h}_{ij} \equiv h_{ij} + 2 \sum_k g_{ijkk}$. This expression is an LCU corresponding to the sparse LCU with $\tilde{h}_{ij}/2$ and $g_{ijkl}/4$ equal to d_q in (39).

The associated MTD representation [Eq. (10)] has $L = 1$, and can be obtained by a trivial $\vec{m} = 1$ index with a single element and no rotation, i.e. $\hat{V}_1 = \hat{1}$. There will be a single $\vec{w} \rightarrow w$ coefficient, thus making the coefficients tensor Ω_w , with the corresponding Ω_w/\hat{p}_w 's running over each of the coefficients/operators appearing in Eq. (40).

A subtle point is that the two-electron component of \hat{H}_e can be expressed by separating $\sigma = \tau$ and $\sigma \neq \tau$ components

$$\begin{aligned} \hat{H}_2 = & \left(\frac{1}{2} \sum_{ij} g_{ijji} \right) \hat{1} \\ & + \frac{1}{4} \sum_{\sigma \neq \tau} \sum_{ijkl} g_{ijkl} \hat{Q}_{ij\sigma} \hat{Q}_{kl\tau} \\ & + \frac{1}{2} \sum_{\sigma} \sum_{i>k, l>j} (g_{ijkl} - g_{ilkj}) \hat{Q}_{ij\sigma} \hat{Q}_{kl\sigma}. \end{aligned} \quad (41)$$

This form of \hat{H}_2 gives lower 1-norms than that in Eq. (40)[31], but it requires separating the spin components and as a consequence twice as many coefficients to be loaded by the PREPARE circuit, making it generally more expensive. Thus, we will always work with the Hamiltonian form shown in Eq. (8), making the two-electron tensor representable using spacial orbitals. In the case where this spin-symmetry is broken, as is the case when obtaining a Hamiltonian from unrestricted Hartree-Fock calculations and generally for any open-shell system, only non-zero coefficients of the two-electron tensor in spin-orbitals need to be loaded. This can be done by using a contiguous register, as shown in Appendix A for the sparse LCU.

2. Anti-commuting groupings

The 1-norm of the Pauli decomposition can be reduced by grouping Pauli products into larger unitaries. Normalized linear combinations of mutually anti-commuting Pauli products yield unitary operators [43] that improve on the 1-norm of (39)

$$\hat{H} = \sum_{n=1}^{N_{AC}} a_n \hat{A}_n, \quad (42)$$

where N_{AC} represents the total number of groups, and

$$a_n \equiv \sqrt{\sum_{q \in K_n} |d_q|^2}, \quad (43)$$

$$\hat{A}_n \equiv \frac{1}{a_n} \sum_{q \in K_n} d_q \hat{P}_q, \quad (44)$$

with \hat{A}_n representing linear combinations of mutually anti-commuting Pauli products, and K_n denoting the associated indices. Within the MTD framework [Eq. (10)], this decomposition has $L = 1$, where \vec{m} takes on a single element such that $\hat{V}_1 = \hat{1}$. The \vec{w} index is identical to the n index in Eq. (42), with $\Omega_n = a_n$ and $\hat{p}_n = \hat{A}_n$. Referring to Eq. (40), we observe that the coefficients d_q associated with products of two Majoranas are purely imaginary, whereas those arising from four Majoranas are real. Considering that products of two Majoranas are anti-Hermitian and products of four Majoranas are Hermitian, it follows that $\hat{A}_n^\dagger = \hat{A}_n$, indicating that \hat{A}_n operators are reflection operators. Lastly, each \hat{A}_n can be implemented using the following equality:

$$\hat{A}_n = \prod_{q \in K_n \uparrow} e^{i\phi_q^{(n)} \hat{P}_q} \prod_{q \in K_n \downarrow} e^{i\phi_q^{(n)} \hat{P}_q}, \quad (45)$$

where \uparrow (\downarrow) denotes ascending (descending) order through K_n , and

$$\phi_q^{(n)} \equiv \frac{1}{2} \arcsin \frac{d_q}{\sqrt{\sum_{i \in K_n, i \leq q} d_i^2}}. \quad (46)$$

Note that this decomposition is the only one presented here in which unitaries can combine both two-Majorana and four-Majorana terms. The application of controlled \hat{A}_n unitaries, as shown in Eq. (45), would require $2|K_n|$ controlled exponentials of Pauli operators, and as a result high T-gate cost. To bring this cost down, we introduce an alternative approach that reduces this number to only

one controlled unitary. The key idea is that for each group K_n , the anti-commutativity of the $|K_n|$ Pauli products generates the Clifford algebra isomorphic to that of the same number of Majorana operators. The key property of a normalized linear combination of N single Majorana operators is that it can be written as a single Majorana conjugated by a sequence of Givens orbital rotations:

$$\sum_n c_n \hat{\gamma}_n = \left(\prod_{n=N-1}^1 e^{\theta_n \hat{\gamma}_n \hat{\gamma}_{n+1}} \right) \hat{\gamma}_1 \left(\prod_{n=1}^{N-1} e^{-\theta_n \hat{\gamma}_n \hat{\gamma}_{n+1}} \right), \quad (47)$$

where the angles θ_n will depend on the c_n 's as

$$\begin{aligned} \theta_1 &= \frac{1}{2} \arccos c_1, \\ \theta_2 &= \frac{1}{2} \arccos \left(\frac{c_2}{\sin 2\theta_1} \right), \\ \theta_3 &= \frac{1}{2} \arccos \left(\frac{c_3}{\prod_{j \leq 2} \sin 2\theta_j} \right), \\ &\vdots \\ \theta_{N-2} &= \frac{1}{2} \arccos \left(\frac{c_{N-2}}{\prod_{j \leq (N-3)} \sin 2\theta_j} \right), \\ \theta_{N-1} &= \frac{\text{sign}(c_N)}{2} \arccos \left(\frac{c_{N-1}}{\prod_{j \leq N-2} \sin 2\theta_j} \right). \end{aligned} \quad (48)$$

Given the identical algebraic structure, the same Givens-based diagonalization can be used to express any unitary consisting of mutually anti-commuting Paulis $\hat{A} \equiv \sum_{j=1}^J a_j \hat{P}_j$:

$$\hat{A} = \left(\prod_{j=J-1}^1 e^{\theta_j \hat{P}_j \hat{P}_{j+1}} \right) \hat{P}_1 \left(\prod_{j=1}^{J-1} e^{-\theta_j \hat{P}_j \hat{P}_{j+1}} \right). \quad (49)$$

By using this expression, the controlled application of each \hat{A}_n only requires a single controlled operation, as shown in the **SELECT** circuit for this LCU in Appendix A.

3. Orbital-optimized qubit operators

1-norm and the number of unitaries for qubit-based decompositions can be reduced further by working with an orbital basis that differs from the canonical molecular orbitals obtained from solving the Hartree-Fock equations. In this study, we explored two distinct orbital rotation schemes: the Foster-Boys orbitals [44] and optimized orbitals obtained by directly minimizing the 1-norm of the

LCU. In both cases, the Hamiltonian is transformed as $\hat{U}^\dagger \hat{H} \hat{U}$, where \hat{U} represents the chosen orbital rotation. This amounts to choosing the Majorana-conserving rotation $\hat{V} = \hat{U}$ instead to $\hat{V} = 1$ in the MTD expression [Eq. (10)]. For the systems studied in Ref. 31, the 1-norm scaling for the Foster-Boys orbitals closely approaches that of the optimal rotations, while requiring $\mathcal{O}(N^3)$ operations to find \hat{U} , as opposed to the $\mathcal{O}(N^5)$ operations needed for finding the 1-norm minimizing rotation.

B. Fermionic LCU decompositions

Next, we illustrate how fermionic-based LCU decompositions can be expressed as MTD. Unitaries in these LCUs are usually constructed as orbital rotations acting on reflections $\hat{Q}_{ii\sigma} \equiv i\hat{\gamma}_{i\sigma,0}\hat{\gamma}_{i\sigma,1} = \hat{1} - 2\hat{n}_{i\sigma}$, where $\hat{n}_{i\sigma} \equiv \hat{a}_{i\sigma}^\dagger \hat{a}_{i\sigma}$ represents the occupation number operator. The fermion-to-qubit mappings transform $Q_{ii\sigma}$ operator to the qubit operator $\hat{z}_{i\sigma}$.

Some methods, particularly those that factorize the g_{ijkl} tensor, separate the one-electron and two-electron operators, which amounts to having separate decompositions for the two-Majorana (\hat{H}_1) and four-Majorana (\hat{H}_2) parts in Eq. (8), with the decomposition for \hat{H}_1 being capped at $L = 2$ and polynomials \hat{p} 's with degree ≤ 2 . Since one-electron operators can be efficiently diagonalized and implemented with an optimal 1-norm [23], any decomposition that treats \hat{H}_1 and \hat{H}_2 separately has an optimal encoding of \hat{H}_1 as

$$\hat{H}_1 = \hat{U}^\dagger \left(\sum_i \mu_i \sum_\sigma \hat{Q}_{ii\sigma} \right) \hat{U}. \quad (50)$$

Note that the most efficient encodings for many fermionic-based decompositions, such as DF and tensor hypercontraction (THC), merge the one- and two-electron coefficients, using a quantum register to indicate whether a given term is coming from one- or two-electron operators [20]. In the case of \hat{H}_2 , the coefficient invariance in the Hamiltonian with respect to spin enables us to decompose the two-electron tensor g_{ijkl} using the spacial-orbital indices, effectively working in the algebra defined by the \hat{F}_j^i operators. Apart from computational efficiency, operating within this spin-symmetric algebra facilitates compilation of the LCU unitaries while requiring less data to be loaded on the quantum computer, as demonstrated in Ref. 20.

1. Single factorization

Although originally deduced with fermionic operators [45], the single factorization (SF) technique can be written with Majoranas as [20, 31]:

$$\hat{H} = c_{\text{SF}} \hat{1} + \frac{i}{2} \sum_{\sigma} \sum_{ij} \tilde{h}_{ij} \hat{\gamma}_{i\sigma,0} \hat{\gamma}_{j\sigma,1} - \frac{1}{4} \sum_{\ell=1}^{N^2} \left(\sum_{\sigma} \sum_{ij} W_{ij}^{(\ell)} \hat{\gamma}_{i\sigma,0} \hat{\gamma}_{j\sigma,1} \right)^2, \quad (51)$$

where $W_{ij}^{(\ell)}$ represents the Cholesky decomposition of the g_{ijkl} tensor written as a $N^2 \times N^2$ matrix g_{ijkl} , and c_{SF} is a constant. We note that the ℓ index is usually truncated at some $M \ll N^2$. Equation (51) illustrates how this decomposition can be cast as an MTD that separates \hat{H}_1 and \hat{H}_2 , with $L = 2$ [Eq. (10)]. The associated sum over \vec{m} has trivial rotations $\hat{V} = \hat{1}$ and M elements. The Majorana polynomials \hat{p} 's correspond to the Majorana products in Eq. (51). Additionally, the complete-square structure of the two-electron elements allows them to be expressed as squares of $\hat{p}_{\ell} \equiv \sum_{\sigma} \sum_{ij} W_{ij}^{(\ell)} \hat{\gamma}_{i\sigma,0} \hat{\gamma}_{j\sigma,1}$ operators. Complete-squares can be encoded through the use of oblivious amplitude amplification, which implements through qubitization the second-degree Chebyshev polynomial of the normalized \hat{p}_{ℓ} , i.e. $2 \left(\hat{p}_{\ell} / N_{\ell}^{(\text{SF})} \right)^2 - \hat{1}$, where the normalization constant $N_{\ell}^{(\text{SF})} \equiv 2 \sum_{ij} |W_{ij}^{(\ell)}|$. Finally, we note that the original procedure did not diagonalize the one-electron term. The MTD representation of single factorization becomes

$$\hat{H} = \tilde{c}_{\text{SF}} \hat{1} + i \sum_{jk\sigma} \Lambda_{jk} \hat{\gamma}_{j\sigma,0} \hat{\gamma}_{k\sigma,1} + \sum_{\ell} \Omega_{\ell} \left(2 \left(\frac{\hat{p}_{\ell}}{N_{\ell}^{(\text{SF})}} \right)^2 - \hat{1} \right), \quad (52)$$

with $\Lambda_{jk} \equiv \frac{h_{jk}}{2} + \sum_l g_{jkl} g_{klj}$, $\Omega_{\ell} \equiv -\frac{(N_{\ell}^{(\text{SF})})^2}{8}$, and \tilde{c}_{SF} has been adjusted to account for the identity term in the Chebyshev polynomials.

2. Double factorization

The DF decomposition [24, 46–51] can be viewed as an extension of SF with the distinction that two-Majorana polynomials are first diagonalized to achieve an optimal 1-norm. In the DF approach, the one-electron term is

diagonalized as shown in Eq. (50). This diagonalization is also used to implement the two-Majorana polynomials \hat{p}_{ℓ} . This approach has $L = 1$ for the MTD [Eq. (10)]. Defining the diagonalized unitaries

$$\begin{aligned} \hat{p}_{\ell} &\equiv i \sum_{ij} W_{ij}^{(\ell)} \sum_{\sigma} \hat{\gamma}_{i\sigma,0} \hat{\gamma}_{j\sigma,1} \\ &= i \hat{U}_{\ell}^{\dagger} \left(\sum_i \mu_i^{(\ell)} \sum_{\sigma} \hat{\gamma}_{i\sigma,0} \hat{\gamma}_{i\sigma,1} \right) \hat{U}_{\ell} \end{aligned} \quad (53)$$

the DF LCU is written in the fermionic representation as

$$\begin{aligned} \hat{H} &= c_{\text{DF}} \hat{1} + \sum_i \mu_i^{(0)} \sum_{\sigma} \hat{U}_0^{\dagger} \hat{Q}_{i\sigma} \hat{U}_0 \\ &+ \sum_{\ell} \left(\sum_i \mu_i^{(\ell)} \sum_{\sigma} \hat{U}_{\ell}^{\dagger} \hat{Q}_{i\sigma} \hat{U}_{\ell} \right)^2, \end{aligned} \quad (54)$$

where c_{DF} is a constant that depends on the μ factors (see Ref. 20). The $\mu^{(l)}$ vectors are obtained by diagonalizing the $W^{(\ell)}$ matrices appearing in the SF approach. This can be recast in the MTD form:

$$\begin{aligned} \hat{H} &= c_{\text{DF}} \hat{1} + i \sum_j \mu_j^{(0)} \sum_{\sigma} \hat{U}_0^{\dagger} \hat{\gamma}_{j\sigma,0} \hat{\gamma}_{j\sigma,1} \hat{U}_0 \\ &+ \sum_{\ell} \Omega_{\ell} \hat{U}_{\ell}^{\dagger} \left(2 \left(\frac{\hat{p}_{\ell}}{N_{\ell}^{(\text{DF})}} \right)^2 - \hat{1} \right) \hat{U}_{\ell}, \end{aligned} \quad (55)$$

with $N_{\ell}^{(\text{DF})} \equiv \sum_i |\mu_i^{(\ell)}|$, $\Omega_{\ell} \equiv \frac{(N_{\ell}^{(\text{DF})})^2}{2}$. For the MTD, \vec{m} runs over $M \leq N^2$ indices. However, \vec{m} is equal to polynomial subscript ℓ (\hat{p}_{ℓ}), which would correspond to an implicit Kronecker delta between \vec{m} and \vec{w} indices (here written as ℓ) in the Ω tensor, with $\hat{V}_{\ell} = \hat{U}_{\ell} \in \text{Spin}(N)$.

3. Cartan sub-algebra

The Cartan sub-algebra (CSA) decomposition generalizes DF to include two-electron terms that are not parts of a complete-square. Thus, it corresponds to a full-rank factorization, as opposed to DF which is known as a low-rank factorization [52–54]. CSA LCU is

$$\begin{aligned} \hat{H} &= c_{\text{CSA}} \hat{1} + \sum_i \mu_i \sum_{\sigma} \hat{U}_0^{\dagger} \hat{Q}_{i\sigma} \hat{U}_0 \\ &+ \sum_{\ell} \sum_{ij} \lambda_{ij}^{(\ell)} \sum_{\sigma\tau} \hat{U}_{\ell}^{\dagger} \hat{Q}_{i\sigma} \hat{Q}_{j\tau} \hat{U}_{\ell}, \end{aligned} \quad (56)$$

where the one-electron term is the same as that appearing in the DF framework. The corresponding MTD form is

$$\hat{H} = c_{\text{CSA}} \hat{1} + i \sum_j \mu_j^{(0)} \sum_{\sigma} \hat{U}_0^\dagger \hat{\gamma}_{j\sigma,0} \hat{\gamma}_{j\sigma,1} \hat{U}_0 - \sum_{\ell,ij} \lambda_{ij}^{(\ell)} \sum_{\sigma\tau} \hat{U}_\ell^\dagger \hat{\gamma}_{i\sigma,0} \hat{\gamma}_{i\sigma,1} \hat{\gamma}_{j\tau,0} \hat{\gamma}_{j\tau,1} \hat{U}_\ell, \quad (57)$$

with $L = 2$ [Eq. (10)]. The associated Ω tensor has an implicit Kronecker delta in the m_1 and m_2 indices. Despite being more flexible than DF, the non-linear optimization procedures required to obtain the Cartan sub-algebra decomposition make its classical computational cost expensive for large systems.

4. Tensor Hypercontraction

The THC decomposition [20, 55] expresses the Hamiltonian as

$$\hat{H} = c_{\text{THC}} \hat{1} + i \sum_j \mu_j \sum_{\sigma} \hat{U}_0^\dagger \hat{Q}_{jj\sigma} \hat{U}_0 + \sum_{\mu\nu} \zeta_{\mu\nu} \sum_{\sigma} \hat{U}_\mu^\dagger \hat{Q}_{11\sigma} \hat{U}_\mu \sum_{\tau} \hat{U}_\nu^\dagger \hat{Q}_{11\tau} \hat{U}_\nu, \quad (58)$$

which corresponds to an $L = 2$ MTD with $\vec{w} = 1$ index [Eq. (10)]. Since the \hat{U} 's orbital rotations are only acting on orbital 1, their implementation requires $\mathcal{O}(N)$ Givens rotations, as opposed to the $\mathcal{O}(N^2)$ required for rotating all orbitals [24]. To better understand this reduction in the number of Givens rotations, we start by noting that for an arbitrary rotation $U \in \text{Spin}(N)$, the maximal torus theorem [56] allows us to write

$$\hat{U} = \prod_{i>j=1}^N e^{\theta_{ij} \hat{F}_j^i}, \quad (59)$$

where the product over Givens rotations can be taken in any order, noting that different sets of θ_{ij} 's will need to be considered for each different ordering. Since $\hat{Q}_{11\sigma}$ only has a component in orbital 1 we can simplify its transformation by leaving only \hat{F}_j^i generators where i or j is 1. To demonstrate validity of this simplification, we use a freedom to choose an order of exponential functions in the \hat{U} product. Such a choice can always be made because generators \hat{F}_j^i form a Lie algebra. The convenient order is to group all Givens rotations not acting on orbital 1 on the left-hand side of \hat{U} ,

$$\begin{aligned} \hat{U}^\dagger \hat{Q}_{11\sigma} \hat{U} &= e^{\theta_{12} \hat{F}_2^1} e^{\theta_{13} \hat{F}_3^1} \dots e^{\theta_{1N} \hat{F}_N^1} \left(\prod_{i>j>1} e^{\theta_{ij} \hat{F}_j^i} \right)^\dagger \hat{Q}_{11\sigma} \\ &\times \left(\prod_{i>j>1} e^{\theta_{ij} \hat{F}_j^i} \right) e^{\theta_{1N} \hat{F}_N^1} \dots e^{\theta_{12} \hat{F}_2^1} \\ &= e^{\theta_{12} \hat{F}_2^1} e^{\theta_{13} \hat{F}_3^1} \dots e^{\theta_{1N} \hat{F}_N^1} \hat{Q}_{11\sigma} \\ &\times e^{\theta_{1N} \hat{F}_N^1} \dots e^{\theta_{12} \hat{F}_2^1}, \end{aligned} \quad (60)$$

where any Givens rotation not involving orbital 1 commutes with $\hat{Q}_{11\sigma}$. Evidently, $N - 1$ Givens rotations are enough for arbitrary orbital rotation of $\hat{Q}_{11\sigma}$.

The corresponding MTD form of the THC decomposition is

$$\begin{aligned} \hat{H} &= c_{\text{THC}} \hat{1} + i \sum_j \mu_j \sum_{\sigma} \hat{U}_0^\dagger \hat{\gamma}_{j\sigma,0} \hat{\gamma}_{j\sigma,1} \hat{U}_0 \\ &+ \sum_{\mu\nu} \zeta_{\mu\nu} \sum_{\sigma} \hat{U}_\mu^\dagger \hat{\gamma}_{1\sigma,0} \hat{\gamma}_{1\sigma,1} \hat{U}_\mu \sum_{\tau} \hat{U}_\nu^\dagger \hat{\gamma}_{1\tau,0} \hat{\gamma}_{1\tau,1} \hat{U}_\nu. \end{aligned} \quad (61)$$

Table I. MTD representation of current LCU's, Pauli and anticommuting (AC) groupings, with their orbital optimized (OO-) versions, correspond to decomposing the full Hamiltonian \hat{H} . All other decompositions separate the one-electron and two-electron components \hat{H}_1 and \hat{H}_2 , with the \hat{H}_2 components shown here and \hat{H}_1 in Eq.(50). Unitaries marked with \hat{U} correspond to real orbital rotations $\in \text{Spin}(N)$. All necessary definitions for operators and constants can be found in the section for the corresponding decomposition.

LCU	L	\vec{m}	$\hat{V}_{\vec{n}}$	\vec{w}	$\Omega_{\vec{w}}^{\vec{m}}$	\hat{p}_{w_k}
Pauli	1	$\vec{m} = 1$	$\hat{V}_1 = \hat{1}$	$\vec{w} = \begin{cases} (i, j, \sigma) \\ (i > k, l > j, \sigma) \end{cases} \rightarrow 2N^2 \rightarrow 2N^4 \rightarrow N^2(N-1)^2$	$\begin{cases} \Omega_{ij\sigma} = \frac{h_{ij}}{2} + \sum_k g_{ijkk} \\ \Omega_{ijkl\sigma} = \frac{g_{ijkl}}{4} \end{cases}$	$\begin{cases} \hat{p}_{jks\sigma} = i\hat{\gamma}_{i\sigma,0}\hat{\gamma}_{j\sigma,1} \\ \hat{p}_{ijkl\sigma} = \hat{\gamma}_{i\sigma,0}\hat{\gamma}_{j\sigma,1}\hat{\gamma}_{k\sigma,0}\hat{\gamma}_{l\sigma,1} \\ \hat{p}_{ijkl\sigma} = \hat{\gamma}_{i\sigma,0}\hat{\gamma}_{j\sigma,1}\hat{\gamma}_{k\sigma,0}\hat{\gamma}_{l\sigma,1} \end{cases}$
AC	1	$\vec{m} = 1$	$\hat{V}_1 = \hat{1}$	$\vec{w} \equiv n = 1, \dots, N_{\text{AC}}$	$\Omega_n = a_n \equiv \sqrt{\sum_{q \in K_n} d_q ^2}$	$\hat{p}_n = \hat{A}_n \equiv \frac{1}{a_n} \sum_{q \in K_n} d_q \hat{P}_q$
OO-Pauli	1	$\vec{m} = 1$	$\hat{V}_1 = \hat{U}_{\vec{\theta}}$	Same as in Pauli	Same as in Pauli	Same as in Pauli
OO-AC	1	$\vec{m} = 1$	$\hat{V}_1 = \hat{U}_{\vec{\theta}}$	Same as in AC	Same as in AC	Same as in AC
SF	1	$\vec{m} = 1$	$\hat{V}_1 = \hat{1}$	$\vec{w} = \ell = 1, \dots, M_{\text{SF}} \leq N^2$	$\begin{cases} \Omega_{\ell} = -\frac{N_{\ell}^{(\text{SF})}}{8} \\ N_{\ell}^{(\text{SF})} = 2 \sum_{ij} W_{ij}^{(\ell)} \\ g_{ijkl} = \sum_{\ell} W_{ij}^{(\ell)} W_{kl}^{(\ell)} \end{cases}$	$\hat{p}_{\ell} + \hat{1} = \left(\frac{\sqrt{2}}{N_{\ell}^{(\text{SF})}} \sum_{ij\sigma} W_{ij}^{(\ell)} \hat{\gamma}_{i\sigma,0} \hat{\gamma}_{j\sigma,1} \right)^2$
DF	1	$\vec{m} = \ell = 1, \dots, M_{\text{DF}} \leq N^2$	$\hat{V}_{\ell} = \hat{U}_{\vec{\theta}_{\ell}} \equiv \hat{U}_{\ell}$	$\vec{w} = \ell = 1, \dots, M_{\text{DF}} \leq N^2$	$\Omega_{\ell} = -\frac{N_{\ell}^{(\text{DF})}}{2}$ $N_{\ell}^{(\text{DF})} = \sum_i \mu_i^{(\ell)} $ $W_{ij}^{(\ell)} = \sum_k \mu_k^{(\ell)} U_{\ell,ik} U_{\ell,jk}$	$\hat{p}_{\ell} + \hat{1} = \left(\frac{\sqrt{2}}{N_{\ell}^{(\text{DF})}} \sum_{i\sigma} \mu_i^{(\ell)} \hat{\gamma}_{i\sigma,0} \hat{\gamma}_{i\sigma,1} \right)^2$
CSA	2	$\vec{m} = \ell = 1, \dots, M_{\text{CSA}}$	$\hat{V}_{\ell} = \hat{U}_{\vec{\theta}_{\ell}} \equiv \hat{U}_{\ell}$	$\vec{w} = (i, j, \sigma, \tau), i\sigma \neq j\tau \rightarrow (4N^2 - 2N)$	$\Omega_{i\sigma j\tau}^{(\ell)} = \lambda_{ij}^{(\ell)}$	$\begin{cases} \hat{p}_{i\sigma}^{(1)} = \hat{\gamma}_{i\sigma,0}\hat{\gamma}_{i\sigma,1} \\ \hat{p}_{j\tau}^{(2)} = \hat{\gamma}_{j\tau,0}\hat{\gamma}_{j\tau,1} \end{cases}$
THC	2	$\vec{m} = (\mu, \nu) \rightarrow M_{\text{THC}}^2$ $\mu, \nu = 1, \dots, M_{\text{THC}}$	$\hat{V}_{\mu} = \hat{U}_{\mu}$	$\vec{w} = (\sigma, \tau) \rightarrow (4)$	$\Omega_{\sigma\tau}^{\mu\nu} = \zeta_{\mu\nu}$	$\begin{cases} \hat{p}_{\sigma}^{(1)} = \hat{\gamma}_{1\sigma,0}\hat{\gamma}_{1\sigma,1} \\ \hat{p}_{\tau}^{(2)} = \hat{\gamma}_{1\tau,0}\hat{\gamma}_{1\tau,1} \end{cases}$
L^4	4	$\vec{m} = m = 1, \dots, W$	$\hat{V}_m^{(\nu)} = \hat{U}_m^{(\nu)}$	$\vec{w} = (\sigma, \tau) \rightarrow (4)$	$\Omega_{\sigma\tau}^{(m)} = \Omega_m$	$\begin{cases} \hat{p}_{\sigma}^{(1)} = \hat{\gamma}_{1\sigma,0} \\ \hat{p}_{\sigma}^{(2)} = \hat{\gamma}_{1\sigma,1} \\ \hat{p}_{\tau}^{(3)} = \hat{\gamma}_{1\tau,0} \\ \hat{p}_{\tau}^{(4)} = \hat{\gamma}_{1\tau,1} \end{cases}$

IV. DISCUSSION

The most time-consuming part of the fault-tolerant QPE algorithm is performing T-gates and their error correction. Considering that the number of applications of the Hamiltonian LCU oracle is proportional to the 1-norm of the used LCU, as a quantum resource cost we use a product of the LCU 1-norm by the number of T-gates required for an implementation of the Hamiltonian oracle. The latter corresponds to the number of T-gates in one **SELECT** and two **PREPARE** operations. We will refer to the quantum resource cost simply as hardness. Additionally, we note that optimizing the compilation strategy for the **SELECT** circuit is imperative for minimizing the hardness. Compilation of these circuits typically exploit structures present in the used LCU *ansatz*, as seen in Ref. 20 for DF and THC approaches which make use of the spin-symmetry that is present (i.e. working with \hat{F}_j^i operators). Whether better circuits can be found for the decompositions that have been introduced in this work is an open question. We note that results for the THC are not shown in this work due to the computational difficulty of performing the associated tensor decomposition in a robust and efficient way.

To assess efficiency of various LCU decompositions we present quantum resource estimates for small molecules (Table II) and 1D hydrogen chains (Fig. 5 and Table III), computational details are provided in Appendix B. Most of LCU methods can be partitioned into three categories based on the small molecule results: 1) low T-gate count and medium 1-norms, Pauli and Pauli-OO; 2) high T-gate count and low 1-norms, AC, OO-AC, and DF; 3) medium T-gate count and high 1-norms, L^4 -CP4 and L^4 -MPS. The only method that combined low 1-norms and low T-gate counts is L^4 -SVD.

Overall, the orbital-optimized Pauli LCU has the lowest hardness in virtue of the small number of T-gates required for its implementation. The **PREPARE** circuit for this decomposition can be optimized to exploit the 8-fold symmetry of the two-electron tensor as shown in Ref. 51, greatly reducing the number of coefficients that need to be loaded. This, along with the simple structure of its **SELECT** circuit make it extremely efficient. For the orbital-optimized schemes in small molecules (Table II) we used the full orbital optimization which minimizes the total 1-norm since the Foster-Boys localization scheme did not improve the results. In contrast, for 1D hydrogen chains, the orbital rotations that minimize the 1-norm yield results similar to those obtained using the Foster-Boys orbital localization scheme, which is in line with findings of Ref. 31. Therefore, for computational efficiency, we used the Foster-Boys localization scheme for the LCUs of hy-

drogen chains. It is worth noting that fermionic-based decompositions, which inherently include orbital rotations as part of the LCU, are unaffected by the orbital basis used to represent the electronic tensor.

Regarding the scaling of hardness with the system size (Table III), the only decomposition which presented a better scaling than Pauli-OO is L^4 -CP4 LCU. We note that extremely large 1-norms were obtained for the L^4 -CP4 tensor decomposition for the small molecules (Table II). We attribute this to an implementation that was used for the CP4 decomposition, and having a more robust implementation will be necessary for larger systems, as discussed in Ref. 58. At the same time, we can see how the L^4 -SVD decomposition gave competitive 1-norms for these molecules, having that both the L^4 -SVD and the L^4 -CP4 decompositions correspond to the same L^4 LCU. On the other hand, the SVD-based 1-norms for the hydrogen chains were larger than their CP4 counterparts, having that the SVD decomposition became prohibitively expensive to compute for the larger chains. Overall, these results establish the L^4 LCU decomposition as a very promising decomposition in terms of hardness; finding the corresponding fragments in a robust and efficient way is work in progress. We believe that this decomposition could be useful for hybrid LCU approaches by obtaining a few large MTD- L^4 fragments before decomposing the rest of the Hamiltonian with some other method. However, exploring these kind of hybrid LCUs is outside the scope of this work.

The anti-commuting (AC) decomposition, when using the orbital optimized Hamiltonians, yielded very competitive 1-norms and requires the fewest qubits. However, the large number of rotations required for its **SELECT** circuit make it require an extremely large number of T-gates, making its hardness one of the worst out of all the studied LCUs. As such, we believe that an implementation of the AC decomposition which loads the Givens rotation angles in the quantum computer could lower significantly the cost compared to the current implementation that we proposed where angles are “hard coded” into the circuits.

The results for the DF shown in this work correspond to the implementation discussed in the Appendix A. The “optimized DF” results in Fig. 5 and Table III correspond to the DF implementation discussed in Ref. 20 where each Toffoli gate has been considered to require 4 T-gates [59]. We note how this decomposition also presents one of the best hardness scalings. However, the number of qubits required for the optimized DF is an order of magnitude larger than that required by other approaches.

The classical pre-processing cost: The Pauli products decomposition of a Hamiltonian has $\mathcal{O}(N^4)$ operators. However, orbital localization schemes can significantly re-

Molecule	$\Delta E/2$	Pauli	OO-Pauli	AC	OO-AC	DF	L^4 -SVD	L^4 -CP4	L^4 -MPS
H_2	1.68	2.54(632)	2.54(632)	2.18(1040)	2.18(1040)	2.11(3792)	2.54(3264)	19.2(3342)	3.80(4658)
LiH	7.72	13.7(1952)	13.0(1944)	10.2(95895)	10.2(93570)	9.78(23671)	10.9(12086)	252.5(9944)	67.9(12226)
BeH_2	16.0	26.4(2144)	25.7(2144)	20.6(99055)	20.6(98214)	20.0(31529)	22.7(15488)	296.3(11796)	144.9(14284)
H_2O	61.5	89.2(2504)	77.4(2480)	71.2(166249)	70.0(166249)	68.9(31529)	72.7(15488)	367.0(11796)	279.5(14284)
NH_3	51.9	84.8(5016)	70.6(3728)	63.0(585623)	61.4(353231)	60.3(39550)	64.5(19548)	889.3(14446)	344.1(16664)

Table II. 1-norms for electronic structure Hamiltonians in the STO-3G basis [57], the numbers of T-gates required to implement the associated Hamiltonian oracle circuit are given in parenthesis. $\Delta E/2$ corresponds to a lower bound for the 1-norm. Pauli: Pauli products as unitaries; AC: anti-commuting grouping technique; OO-prefix indicates that orbitals were optimized to minimize the 1-norm; DF: double factorization; L^4 -SVD, L^4 -CP4, and L^4 -MPS: MTD- L^4 decompositions introduced in Sec. II A 1.

duce this to $\mathcal{O}(N^2)$ for large molecules [60]; the cost for optimized orbital localization schemes typically scales as $\mathcal{O}(N^3)$ [31]. The sorted insertion algorithm, used in AC, has a sorting cost of $\mathcal{O}(M^2)$, where M is the number of elements in the list being sorted. This results in a decomposition cost of $\mathcal{O}(N^8)$ for AC and $\mathcal{O}(N^4)$ when grouping is done on localized orbitals. For the fermion-based methods, the cost for DF is dominated by the diagonalization of the reshaped $N^2 \times N^2$ tensor $g_{ij;kl}$, which scales as $\mathcal{O}(N^6)$. For the L^4 -MPS, the cost for each step in the MPS factorization (see Fig. 3) goes as $\mathcal{O}(N^5)$, thus being the overall scaling cost of this decomposition. The L^4 -SVD decomposition quickly becomes prohibitively expensive to do as the system size grows, while the L^4 -CP4 decomposition requires $\mathcal{O}(N^3W)$, where W is the number of terms in the decomposition [58]. Among the algorithms presented in this work, orbital-localized AC has the best theoretical scaling, followed by L^4 -MPS. However, in practice, the fermionic-based decompositions (DF and L^4 -MPS) tend to have lower prefactors due to their efficient utilization of linear algebra routines. For example, in the case of the linear H_{30} chain, orbital-localized AC took approximately 5 minutes, while DF required around 0.1 seconds and L^4 -MPS required around 0.3 seconds. These calculations were done using a single core of a 2.2 GHz 6-Core Intel i7 processor.

In summary, this work has introduced the MTD framework, which provides a unified approach to LCU decompositions of the electronic structure Hamiltonian. This framework not only presents a unifying perspective but also leads to the MTD- L^4 decomposition, which expresses the electronic structure tensor as a minimal-rank representation. This decomposition establishes a connection between popular tensor decompositions and LCUs. A study over small systems revealed the LCU based on Pauli products with an orbital optimization to be the most competitive. However, the MTD- L^4 decomposition had bet-

ter scaling coefficients, suggesting that as we go to larger systems this decomposition could be more efficient to implement.

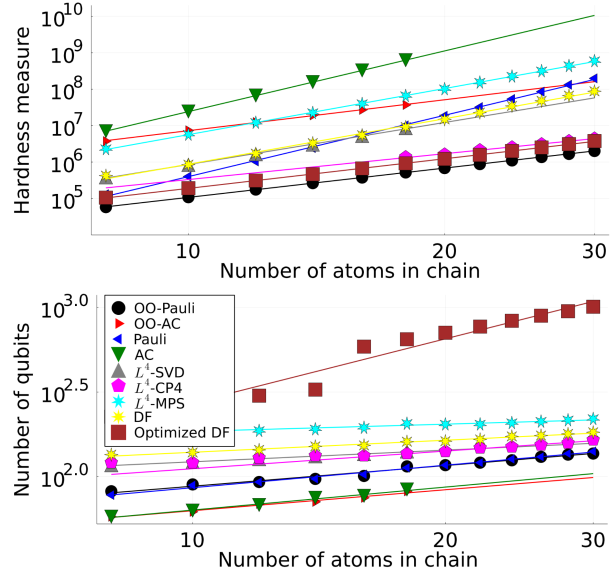


Figure 5. Hardness (top) and the number of qubits (bottom) scaling for different LCUs for hydrogen chains with N atoms with a spacing $r = 1.4 \text{ \AA}$. Hardness is defined as the product of the 1-norm λ with the number of T-gates for one `SELECT` and two `PREPARE` oracles. Lines correspond to a least-square fit, $\log_{10} y = \alpha + \beta \log_{10} x$. Coefficients α and β are reported in Table III. Orbital optimizations were done using the Foster-Boys localization [44].

ACKNOWLEDGEMENTS

We are grateful to Nathan Wiebe and Nicholas Rubin for valuable discussions. I.L. and A.F.I. gratefully appreciate financial support from the Mitacs Elevate Postdoctoral Fellowship and Zapata Computing Inc.

LCU method	Fitted quantity	α	β
Pauli	$\lambda \times \#T\text{-gates}$	0.01	5.59
	# qubits	1.49	0.44
AC	$\lambda \times \#T\text{-gates}$	1.85	5.53
	# qubits	1.35	0.45
OO-Pauli	$\lambda \times \#T\text{-gates}$	2.36	2.67
	# qubits	1.54	0.41
OO-AC	$\lambda \times \#T\text{-gates}$	4.04	2.82
	# qubits	1.39	0.41
L^4 -SVD	$\lambda \times \#T\text{-gates}$	2.10	3.83
	# qubits	1.86	0.23
L^4 -CP4	$\lambda \times \#T\text{-gates}$	3.17	2.36
	# qubits	1.85	0.23
L^4 -MPS	$\lambda \times \#T\text{-gates}$	2.55	4.20
	# qubits	2.12	0.14
DF	$\lambda \times \#T\text{-gates}$	1.80	4.14
	# qubits	1.91	0.24
Optimized DF	$\lambda \times \#T\text{-gates}$	2.58	2.70
	# qubits	0.66	1.75

Table III. Linear fit coefficients for Fig. 5, $\log_{10} y = \alpha + \beta \log_{10} x$.

Appendix A: LCU circuits

In this section we give an overview of all the necessary components for the PREPARE and SELECT circuits for the different LCUs. Most of these circuits have been developed in Refs.20, 24, 29, here, we include circuits that have not been explicitly drawn before, along with those corresponding to the newly proposed LCUs in this work. We make extensive use of the QROM and unary iteration circuits shown in Ref. 29, these procedures are denoted on our circuit diagrams as “*In*” and “data” directives, respectively. Note that usage of a more advanced version of QROM, i.e. QROAM [61], could improve the circuits by modifying the T-gate and ancilla counts. However studying the additional benefits of this technique are beyond the scope of this work. In all the shown circuits, we use the convention where having a single-qubit gate (e.g., Hadamard) applied to a multi-qubit register corresponds to applying that gate on each of the qubits of the register. An overview of the resource cost for all circuits is given in Table IV, with pertinent parameters defined either in the Table IV caption or in the associated circuit in this section.

Table IV. T-gate, number of logical qubits, and number of controlled R_Z rotations cost of quantum circuits of interest for this work. Reusable qubits corresponds to those that are left in the $|0\rangle$ state after the directive is executed, and is also included in the logical qubit count. We have used $b_n \equiv \lceil \log_2 n \rceil$, $k_n \equiv \lfloor \log_2 n \rfloor$, and $l_n \equiv \lceil \log_2(n/(2^{k_n})) \rceil$ such that $b_n = k_n + l_n$. $\mu_n \equiv \lceil \log_2(n\epsilon) \rceil$ corresponds to the number of bits required for the ‘‘alt’’ register used when preparing a coherent superposition of n coefficients with an accuracy of ϵ . In general, ϵ corresponds to the target accuracy for the given directive and λ to the 1-norm of the LCU. N represents the number of spacial orbitals. Numbers in braces for PREPARE circuit correspond to additional resources when circuits are controlled by an additional qubit, shown by the $|ct\rangle$ register in the corresponding figures. We always consider all SELECT operations to be controlled by a $|ct\rangle$ qubit. All constants are defined in the caption of the corresponding figure. As shown in Ref. 62, R_Z rotations can be optimally implemented for a target accuracy $\epsilon < 0.016$ with an average T-gate cost of $3.067 * \log_2(1/\epsilon) + 9.678$ and one additional reusable qubit. The controlled Givens(N) directive corresponds to an orbital rotation consisting of $N - 1$ Givens rotations that are controlled by a register where the corresponding angles have been previously loaded, as shown in Refs. 20, 24. The rotations for this directive can be implemented using the phase gradient technique [63] for a cost no larger than 7 T-gates per rotation. Note that our notation for N differs by a factor of 2 to that in Ref. 20.

Circuit directive	T-gates complexity ($\#T$)	Number of non reusable qubits ($\#Q$)	Number of reusable qubits ($\#R_Q$)	R_Z complexity ($\#R_Z$)
UNIFORM(K) (Ref. [29])	$8l_K + \{2l_K + 2k_K\}$	$k_K + l_K + \{1\}$	l_K	2
Controlled SWAP($b \leftrightarrow b$)	$7b$	$2b + 1$	0	0
Controlled Givens(N)	$\beta \equiv \lceil 5.652 + \log_2 N \lambda / \epsilon \rceil$	$N + \beta + 1$	0	0
PREP(K) (Fig. 6)	$8l_K + 4K + 8\mu_K + 7b_K - 8 + \{4 + 2k_K + 2l_K\}$	$b_K + 2\mu_K + 3 + \{1\}$	$\#Q(\text{PREP}(K)) + 2$	2
PREP _V (K) (Fig. 7)	$\#T(\text{PREP}(K)) + 7$		$\#Q(\text{PREP}(K)) + 2$	2
PREP(Sparse) (Fig. 8)	$8l_S + 4S + 8\mu_S + 56b_N - 1$	$b_S + 8b_N + 2\mu_S + 8$	$\max[l_S; b_S - 1; 2\mu_S - 1]$	2
SEL(Sparse) (Fig. 10)	$32N - 16$	$4b_N + 4 + 2N$	$b_{2N} + 1$	0
PREP(AC) (Fig. 11)	$\#T(\text{PREP}(G))$	$\#Q(\text{PREP}(G))$	$\#R_Q(\text{PREP}(G))$	2
SEL(AC) (Fig. 11)	$4G - 4$	$2N + b_G + 1$	b_G	$2(\sum_n G_n) - 2G$
PREP(L^4)	$\#T(\text{PREP}(W))$	$\#Q(\text{PREP}(W))$	$\#R_Q(\text{PREP}(W))$	2
SEL(L^4) (Fig. 14)	$N(112\beta - 196) + 8W - 4$	$4 + b_W + 2N + 4\beta$	b_W	0
PREP(L^4 -MPS) (Fig. 9)	$\#T(c\text{PREP}(N)) + \#T(c\text{PREP}(\alpha_1)) + 13 + b_N + b_{\alpha_2} + b_{\alpha_3} + 2\mu_N + 2\mu_{\alpha_1} + 2\mu_{\alpha_2} + 2\mu_{\alpha_3}$	$4 + b_{\alpha_2} + 2\mu_{\alpha_2}$		9
SEL(L^4 -MPS) (Fig. 15)	$4\alpha_2(N + 2\alpha_1 + 2\alpha_3) + N(112\beta - 192) + 8\alpha_1 + 4\alpha_3 - 24$	$b_{\alpha_2\alpha_3}$		0
PREP(DF) (Fig. 13)	$L(8 + 40l_N + 16N + 32\mu_N + 28b_N + 8\kappa_N) + N(28\beta - 48) + 4b_N - 20$	$7 + \beta + 3b_N + b_L + \max[2\mu_N - 1; b_N - 1; l_N]$		$8L$

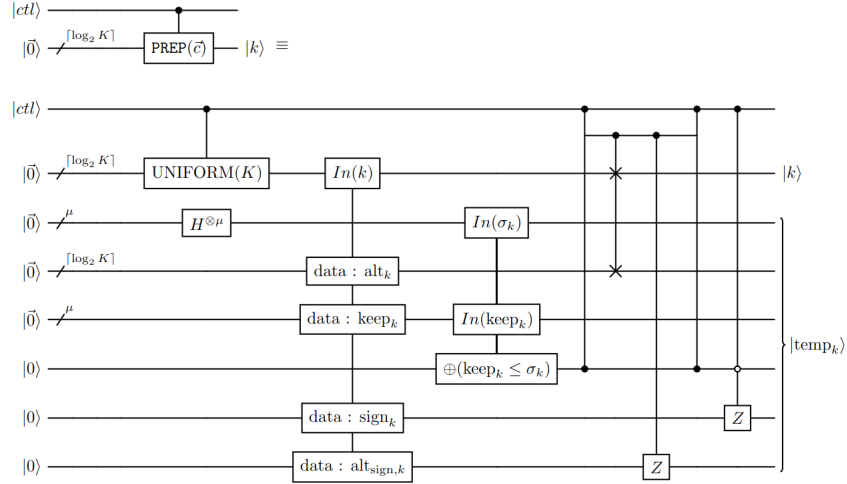


Figure 6. Generic PREPARE : controlled coherent state preparation circuit for a coefficient vector $\vec{c} \equiv (c_0, c_1, \dots, c_{K-1})$, as shown in a non-controlled version in Fig. 11 of Ref. 29. The coefficients c_k are implemented with a μ -bit approximation \tilde{c}_k such that $|c_k - \tilde{c}_k| \leq 1/2^\mu K$. For calculating the complexity of this circuit, we have defined l and L such that $K = 2^l L$ where L is an odd number different than 1, noting that for $L = 1$ we only need to apply Hadamard gates to implement the uniform superposition. The alt and keep values can be obtained from specifying \vec{c} and μ , as shown in Ref. 29.

1. PREPARE circuits

Here we discuss the PREPARE circuits for all LCUs shown in this work that have not been explicitly drawn in the past. The circuit labeled as UNIFORM(K) will be used throughout, it prepares an equal superposition over K states with accuracy ϵ , and is shown in Fig. 12 of Ref. 29. We have also included the sign preparation routine in these circuits, making the output prepare the coefficients with their corresponding signs. A general PREPARE circuit for an arbitrary coefficient is shown in Fig. 6, which can be used to implement the AC PREPARE oracle. A PREPARE circuit that additionally prepares a V register that is used for flagging the one-electron terms, is shown in Fig. 7; this circuit can be used for the CP4 decomposition. Circuits for THC are discussed in Ref. 20.

The quantum resource components for the generic PREPARE (Fig. 6) are:

- uniform superposition over K states, using two R_Z 's, and $8l_K$ T-gates, where $K = l_K 2^{k_K}$ for the largest possible integer k_K such that $l_K \geq 1$ (This operation requires l_K reusable qubits.)
- QROM over K indices, requiring $4(K - 1)$ T-gates and $b_K - 1$ reusable qubits
- arithmetic gate over the keep and σ registers, requiring $4(2\mu_K - 1)$ T-gates and $2\mu_K - 1$ reusable qubits
- one controlled swap gate on the prepare and alt registers, requiring $7b_K$ T-gates
- Hadamard and controlled Z operations with no fault-tolerant cost contributions
- if the circuit is applied in a controlled manner, the uniform superposition uses an additional $2l_K + 2k_K$ number of T-gates; we also require one additional reusable qubit, and 4 extra T-gates for the register with the And operation between the additional control register and the arithmetic operation register.

Considering all of these operations, the total cost parts for the generic PREPARE circuit are:

- $8l_K + 4(K - 1) + 4(2\mu_K - 1) + 7b_K = 8l_K + 4K + 8\mu_K + 7b_K - 8$ T-gates
- $b_K + 2\mu + 3$ non-reusable qubits

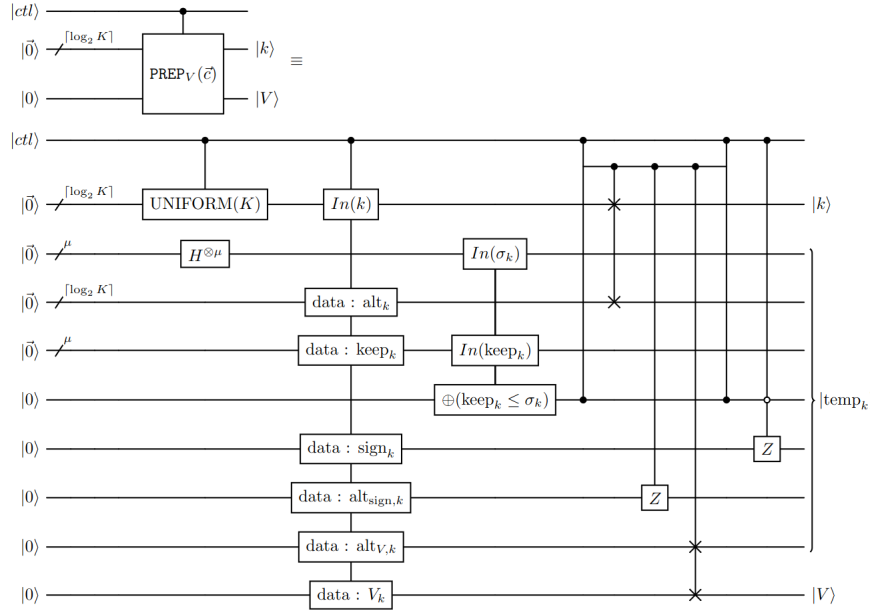


Figure 7. Coherent state preparation that also prepares a qubit register V for flagging a particular set of coefficients, e.g., one-electron coefficients.

- $\max[l_K, b_K - 1, 2\mu_K - 1]$ reusable qubits
- 2 R_Z rotations
- additional $2l_K + 2k_K + 4$ T-gates, one non-reusable qubit, and one reusable qubit, if the operation is controlled.

For the generic PREPARE where we also have the V register, the cost is the same as for the generic PREPARE , with two additions:

- one controlled swap for a cost of 7 T-gates
- two additional non-reusable qubits.

Sparse Pauli

The PREPARE circuit for the Pauli LCU can be implemented efficiently by exploiting the sparsity of the g_{ijkl} tensor [51]. The corresponding circuit is shown in Fig. 8. The symmetry of the electronic tensors has been used for reducing

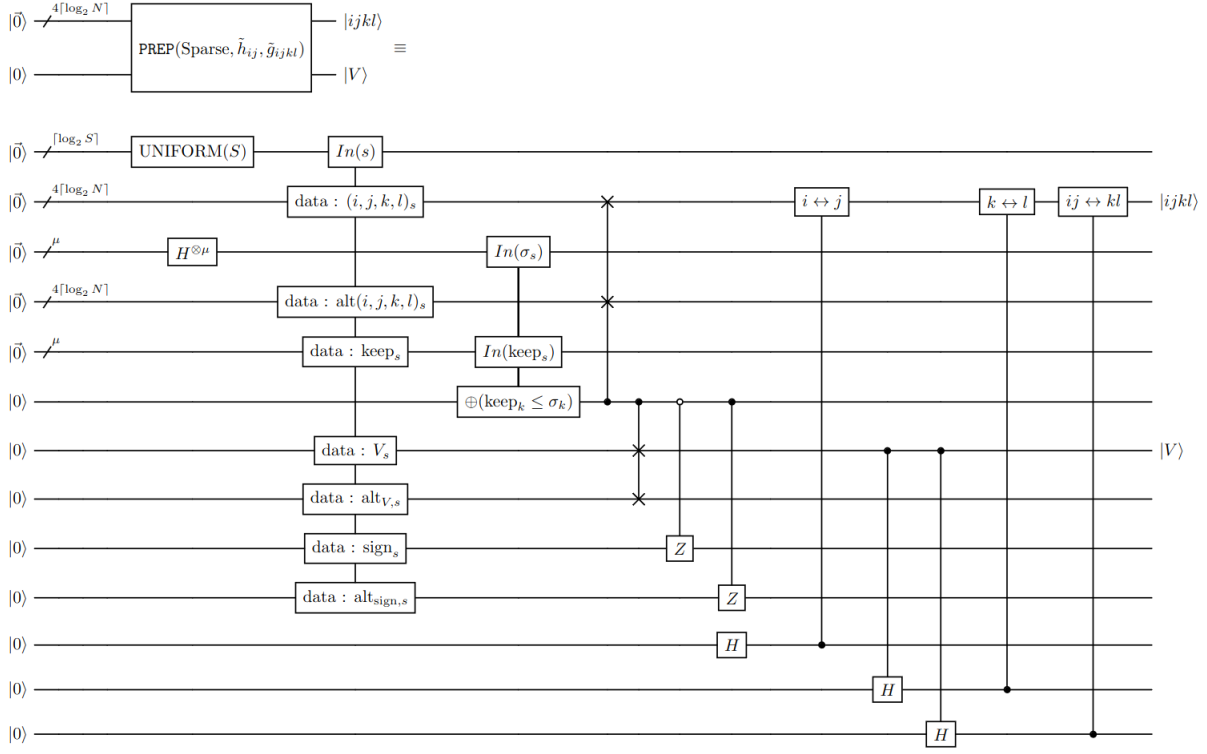


Figure 8. Sparse state preparation circuit for coefficient tensors h_{ij} and \tilde{g}_{ijkl} , as discussed in Ref. 51. We create a coefficient vector with length S and values corresponding to the non-zero entries of $\zeta_{ij}h_{ij}$ and $\zeta_{ij}\zeta_{kl}\zeta_{ijkl}\tilde{g}_{ijkl}$ for defining keep_s , which also defines the set of indices $(V, i, j, k, l)_s$ that are used for the index-loading and alt routines. Thus, only non-zero entries are loaded by QROM, along with the corresponding indices for i, j, k, l , and V which indicates if the coefficient comes from h_{ij} or \tilde{g}_{ijkl} for $V = 0, 1$ respectively. The controlled swap operations in the i, j, k, l register swap between these registers as respectively indicated by the parenthesis on top of the crosses.

the amount of data to load, having defined the auxiliary variables

$$\zeta_{ij} \equiv \begin{cases} \sqrt{2}, & i < j, \\ 1, & i = j, \\ 0, & i > j, \end{cases} \quad (A1)$$

$$\zeta_{ijkl} \equiv \begin{cases} \sqrt{2}, & i < k \text{ or } i = k \text{ and } j < l \\ 1, & i = k \text{ and } j = l \\ 0, & i > k \text{ or } i = k \text{ and } j > l \end{cases} \quad (A2)$$

$$\tilde{g}_{ijkl} \equiv \begin{cases} 1, & |g_{ijkl}| \geq \epsilon_{\text{sparse}}, \\ 0, & |g_{ijkl}| < \epsilon_{\text{sparse}}, \end{cases} \quad (A3)$$

where we have judiciously assigned the tolerance $\epsilon_{\text{sparse}} = 1 \times 10^{-5}$. By using these definitions, only 1/2 and 1/8 of the coefficients need to be loaded on the quantum computer, for the one- and two-electron tensors respectively.

The circuit quantum resources for the sparse PREPARE circuit are:

- uniform superposition over S coefficients, requiring $2 R_Z$, $8l_S$ T-gates, and l_S reusable qubits
- QROM over S indices, requiring $4(S - 1)$ T-gates and $b_S - 1$ reusable qubits

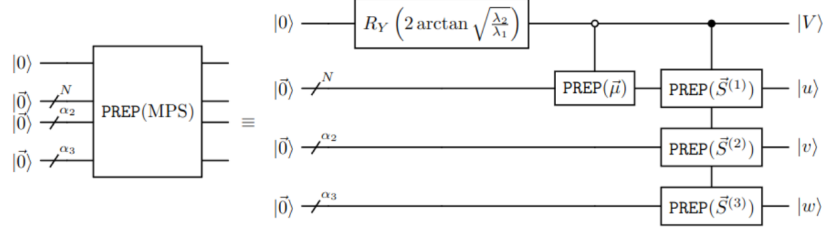


Figure 9. PREPARE circuit for MPS decomposition. λ_1 and λ_2 correspond respectively to the 1-norm of the one- and two-electron components. $\vec{\mu}$ corresponds to the vector with the components of the one-electron operator after diagonalization. The $\vec{S}^{(i)}$ coefficients are obtained with the nested SVD for obtaining the MPS, as shown in Eq. (19)

- arithmetic gate, requiring $4(2\mu_S - 1)$ T-gates and $2\mu_S - 1$ reusable qubits
- controlled swaps, requiring in total $7(4b_N + 1 + b_N + b_N + 2b_N) = 56b_N + 7$ T-gates
- controlled Z's and Hadamard gates, for no additional fault-tolerant cost.

The total cost components of the sparse PREPARE circuit then becomes

- $8l_S + 4(S - 1) + 4(2\mu_S - 1) + 56b_N + 7 = 8l_S + 4S + 8\mu_S + 56b_N - 1$ T-gates.
- $b_S + 8b_N + 2\mu_S + 8$ non-reusable qubits.
- $\max[l_S, b_S - 1, 2\mu_S - 1]$ reusable qubits.
- 2 R_Z rotations.

a. Matrix Product States

The structure of the MPS decomposition makes it amenable to a more optimal PREPARE circuit than that of the L^4 decomposition, and is shown in Fig. 9. The associated circuit quantum resources are:

- one R_Z rotation gate
- one controlled generic PREPARE circuit over N indices
- three controlled generic PREPARE circuits over respectively α_1 , α_2 , and α_3 indices.

The total cost for this circuit parts are:

- $\sum_A (10l_A + 2k_A + 4A + 8\mu_A + 7b_A - 4)$ T-gates, where $A = N, \alpha_1, \alpha_2, \alpha_3$
- $1 + b_N + b_{\alpha_2} + b_{\alpha_3} + \sum_A (2\mu_A + 3)$ non-reusable qubits
- $4 + b_{\alpha_2} + 2\mu_{\alpha_2}$ reusable qubits
- 9 R_Z rotations.

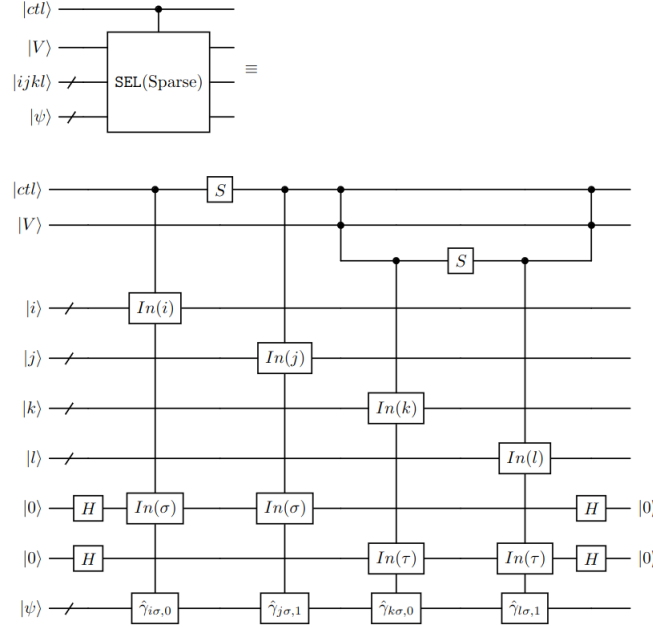


Figure 10. Controlled SELECT circuit for Pauli (or sparse) decomposition. An optimal implementation of the multiplexed Majorana operators is shown in Ref. 29.

2. SELECT circuits

We now illustrate how the SELECT circuits of the different LCUs can be implemented. The circuits for the THC decomposition and the most optimized version of DF are shown in Ref. 20. We note that all SELECT circuits shown here are controlled by a control register, as required for the implementation of the qubitized walk operator. All required inputs for these circuits are given as an output by the PREPARE oracles. The $|\psi\rangle$ register encodes the electronic wavefunction over all $2N$ spin orbitals, while $|\psi_{\uparrow}\rangle/|\psi_{\downarrow}\rangle$ corresponds to the register with only up/down spins and thus having N qubits.

a. Sparse Pauli

The SELECT circuit for the sparse LCU is shown in Fig. 10. The circuit complexity for this SELECT circuit is:

- 4 controlled Majorana operations over $2N$ indices, each one requiring $4(2N - 1)$ T-gates and b_{2N} reusable qubits.
- One *And* operation, requiring 4 T-gates and one reusable qubit.
- All the Hadamards and S-gates can be implemented without a fault-tolerant cost.

The total cost of the circuit then becomes

- $32N - 16$ T-gates.
- $4b_N + 4 + 2N$ non-reusable qubits.
- $b_{2N} + 1$ reusable qubits.

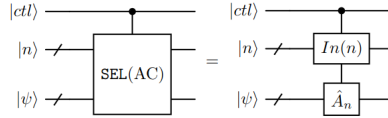


Figure 11. SELECT oracle for the AC LCU, which used unary iteration over n index. The circuit for each controlled \hat{A}_n unitary is shown in Fig. 12.

b. Anti-commuting groups of Pauli products

The Givens-based diagonalization for implementing the unitaries coming from the AC grouping is discussed in Sec. III A 2. The SELECT circuit for AC is then shown in Fig. 11. The associated cost for this circuit is

- one controlled unary iteration over G indices, requiring $4(G - 1)$ T-gates and b_G reusable qubits
- G controlled \hat{A}_n operators, each one requiring two Givens diagonalization circuits over G_n terms and a controlled Pauli with no fault-tolerant cost. (Each Givens diagonalization circuit requires $G_n - 1$ controlled R_Z when using the staircase algorithm for implementing exponentials of Pauli products [64].)

The total cost for this SELECT circuit is:

- $4G - 4$ T-gates
- $b_G + 1 + 2N$ non reusable qubits
- b_G reusable qubits
- $2(\sum_n G_n) - 2G$ controlled R_Z rotations.

c. Double factorization

The double factorization circuit can be implemented in different ways. First proposed in Ref. 24, a more efficient implementation was then proposed in Ref. 20. However, the resulting circuits for the latter are significantly harder to analyze. As such, in this work we propose a hybrid implementation, which is based on that of Ref. 24 with the only difference that both one- and two-electron terms are implemented in the same circuit by having a qubit flagging the one-electron part, as done in Ref. 20. The associated cost components to implement this circuit are:

- 6 QROM circuits over L indices, requiring $24(L - 1)$ T-gates and b_L reusable qubits, here $L = M_{DF} + 1$
- 2 multiplexed Givens rotation circuits, each one requiring $14N(\beta - 2)$ T-gates
- $4L$ controlled PREPARE circuits over N coefficients, each one requiring $10l_N + 4N + 8\mu_N + 7b_N - 4 + 2k_N$ T-gates, $b_N + 2\mu_N + 4$ non-reusable qubits, $\max[2\mu_N - 1; b_N - 1; l_N] + 1$ reusable qubits, and 2 R_Z rotations (Note that the non-reusable qubits can be shared for all these PREPARE circuits)
- 4 Hadamard gates, for no fault-tolerant cost
- 2 controlled QROMs over N indices, requiring $8N$ T-gates and $b_N + 1$ reusable qubits
- one Z gate multi-controlled by b_N qubits, requiring $4b_N$ T-gates and $b_N - 1$ reusable qubits
- one *And* gate, requiring 4 T-gates and one reusable qubit.

The total complexity for the DF SELECT circuit is:

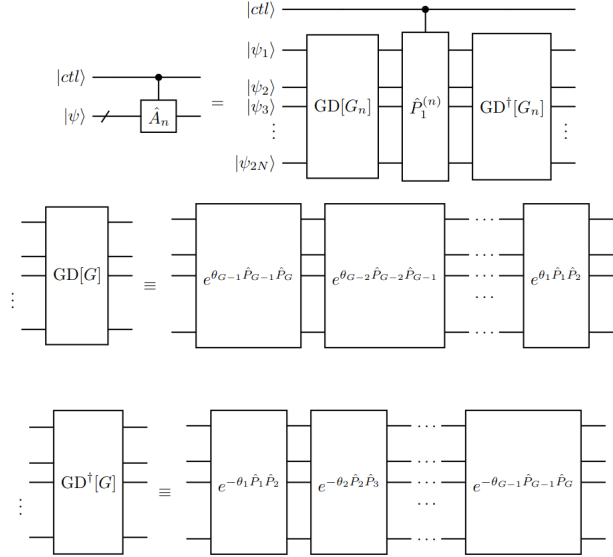


Figure 12. Circuit for implementing a controlled \hat{A}_n unitary for the AC decomposition (top). The associated Givens diagonalization unitaries are shown in the middle and in the bottom. Here, G_n corresponds to the n -th group of mutually AC Pauli products, with $P_k^{(n)}$ its k -th element.

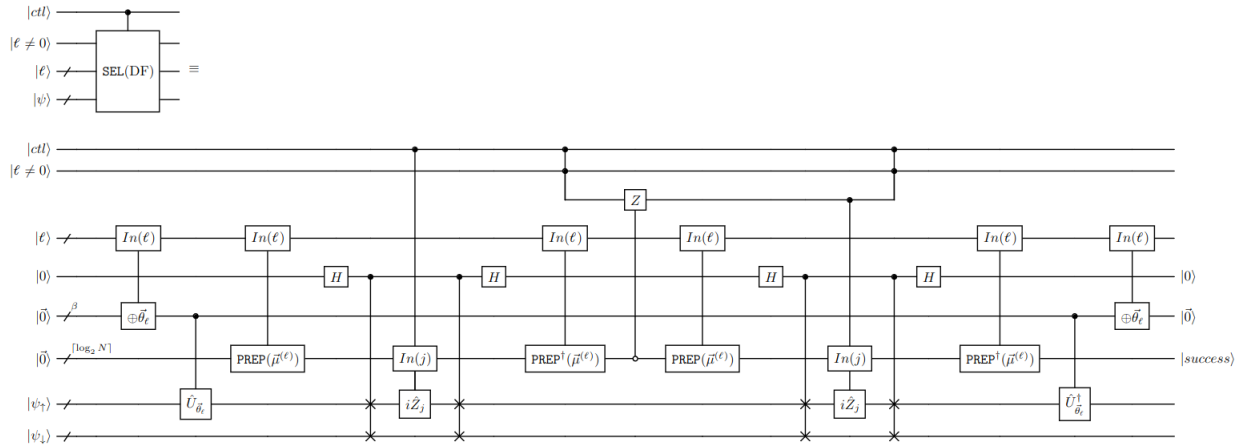


Figure 13. Circuit for implementing a **SELECT** oracle of double factorized LCU. Note how each of the unitaries depending on $|\ell\rangle$ is implemented by block-encoding. The register with the $|success\rangle$ encodes whether the application of these block-encodings was successful.

- $24(L-1) + 28N(\beta-2) + 4L(10l_N + 4N + 8\mu_N + 7b_N - 4 + 2k_N) + 8N + 4b_N + 4 = L(8 + 40l_N + 16N + 32\mu_N + 28b_N + 8k_N) + N(28\beta - 48) + 4b_N - 20$ T-gates
- $6 + b_L + 2N + b_N + 2\mu_N$ non-reusable qubits
- $2 + \beta + b_N + b_L + \max[2\mu_N - 1; b_N - 1; l_N] + 1 + b_N + 1 + b_N - 1 + 4 = 7 + \beta + 3b_N + b_L + \max[2\mu_N - 1; b_N - 1; l_N]$ reusable qubits

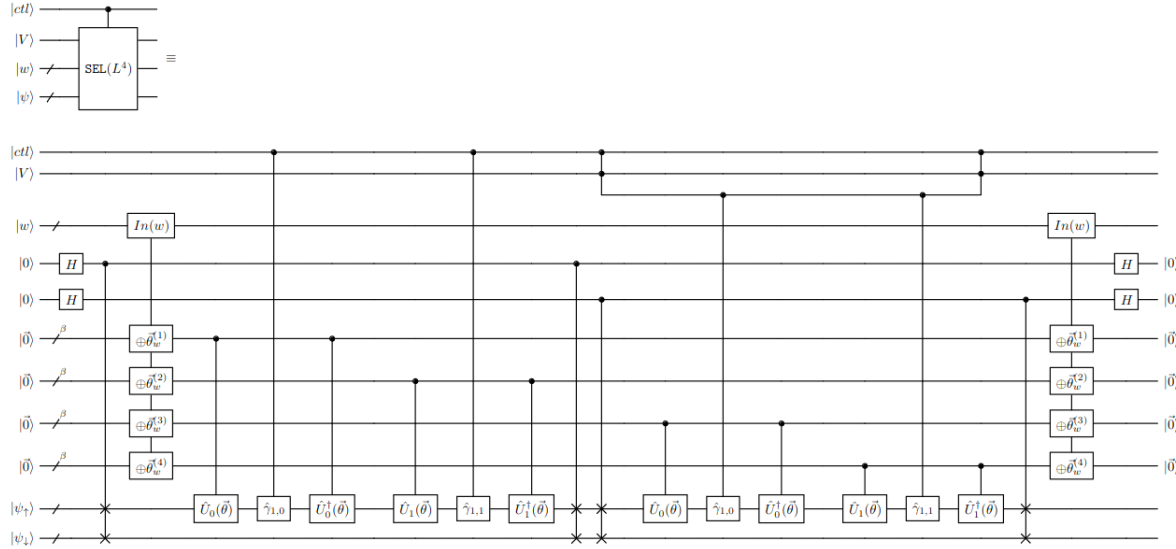


Figure 14. SELECT circuit for implementing MTD- L^4 LCU.

- $8L R_Z$ rotations.

d. MTD- L^4 decomposition

The implementation of the SELECT circuit for the MTD- L^4 decomposition is shown in Fig. 14. This implementation minimizes the T-gate count in exchange for a higher number of ancilla qubits: four registers are used simultaneously for loading the Givens rotation angles, minimizing the number of times QROM must be called for angle loading. The cost for the MTD- L^4 SELECT circuit is:

- 4 controlled swaps with an individual cost of $7N$ T-gates
- 2 QROM circuits over W indices, each one requiring $4(W - 1)$ T-gates and $b_W - 1$ reusable qubits
- 8 multiplexed Givens rotations circuits, each requiring $14N(\beta - 2)$ T-gates
- one *And* operation, requiring 4 T-gates and one reusable qubit
- controlled single Majoranas, along with the Hadamard gates, which have no fault-tolerant cost.

The total complexity for the MTD- L^4 SELECT circuit is:

- $4 * 7N + 2 * 4(W - 1) + 8 * 14N(\beta - 2) + 4 = N(112\beta - 196) + 8W - 4$ T-gates
- $4 + 2N + b_W + 4\beta$ non-reusable qubits
- b_W reusable qubits.

e. Matrix Product States

The SELECT circuit for the L^4 -MPS can be seen in Fig. 15. The associated complexity components are:

- one QROM over $N + \alpha_1$ indices, requiring $4(N + \alpha_1 - 1)$ T-gates and $b_{N+\alpha_1} - 1$ reusable qubits
- one controlled QROM over $\alpha_1\alpha_2$ indices, requiring $4(\alpha_1\alpha_2 - 1)$ T-gates and $b_{\alpha_1\alpha_2}$ reusable qubits
- one QROM over $(N + \alpha_1)\alpha_2$ indices, requiring $4((N + \alpha_1)\alpha_2 - 1)$ T-gates and $b_{(N+\alpha_1)\alpha_2} - 1$ reusable qubits
- two QROMs over $\alpha_2\alpha_3$ indices, each one requiring $4(\alpha_2\alpha_3 - 1)$ T-gates and $b_{\alpha_2\alpha_3} - 1$ reusable qubits
- one QROM over α_3 indices, requiring $4(\alpha_3 - 1)$ T-gates and $b_{\alpha_3} - 1$ reusable qubits
- 4 controlled swap gates, each one requiring $7N$ T-gates/
- 8 multiplexed Givens rotations circuits, each requiring $14N(\beta - 2)$ T-gates
- one *And* gate for 4 T-gates and one reusable qubit
- controlled single Majoranas and Hadamard gates for no additional fault-tolerant cost.

The total complexity for the MPS SELECT circuit then becomes

- $4(N + \alpha_1 + \alpha_1\alpha_2 + (N + \alpha_1)\alpha_2 + 2\alpha_2\alpha_3 + \alpha_3 - 6) + 4 * 7N + 8 * 14N(\beta - 2) + 4 = N(4\alpha_2 + 112\beta - 192) + \alpha_2(8\alpha_1 + 8\alpha_3) + 8\alpha_1 + 4\alpha_3 - 24$ T-gates
- $4 + 2N + \beta + b_N + b_{\alpha_2} + b_{\alpha_3}$ non-reusable qubits
- $b_{\alpha_2\alpha_3}$ reusable qubits.

Appendix B: Computational details

All electronic Hamiltonians in the minimal STO-3G basis set were obtained with the PySCF [65–67] package. Results involving tensor decompositions of two-electron integrals correspond to the lowest rank sufficient to obtain a converged two-electron tensor with the 2-norm error $\sum_{ijkl} |\Delta g_{ijkl}|^2$ below 1×10^{-6} . All LCU decompositions were done using the QuantumMAMBO package on Julia, which is available at <https://github.com/iloaiza/QuantumMAMBO.jl>.

Molecular geometries

For the molecules in Table II, the nuclear configurations are:

- $R(H - H) = 0.741\text{\AA}$ for H_2
- $R(Li - H) = 1.595\text{\AA}$ for LiH
- $R(Be - H) = 1.326\text{\AA}$ with a collinear atomic arrangement for BeH_2
- $R(O - H) = 0.958\text{\AA}$ with angle $\angle HOH = 107.6^\circ$ for H_2O
- $R(N - H) = 1\text{\AA}$ with $\angle HNH = 107^\circ$ for NH_3

For the hydrogen chains, the $R(H - H)$ distance was taken to be 1.4\AA .

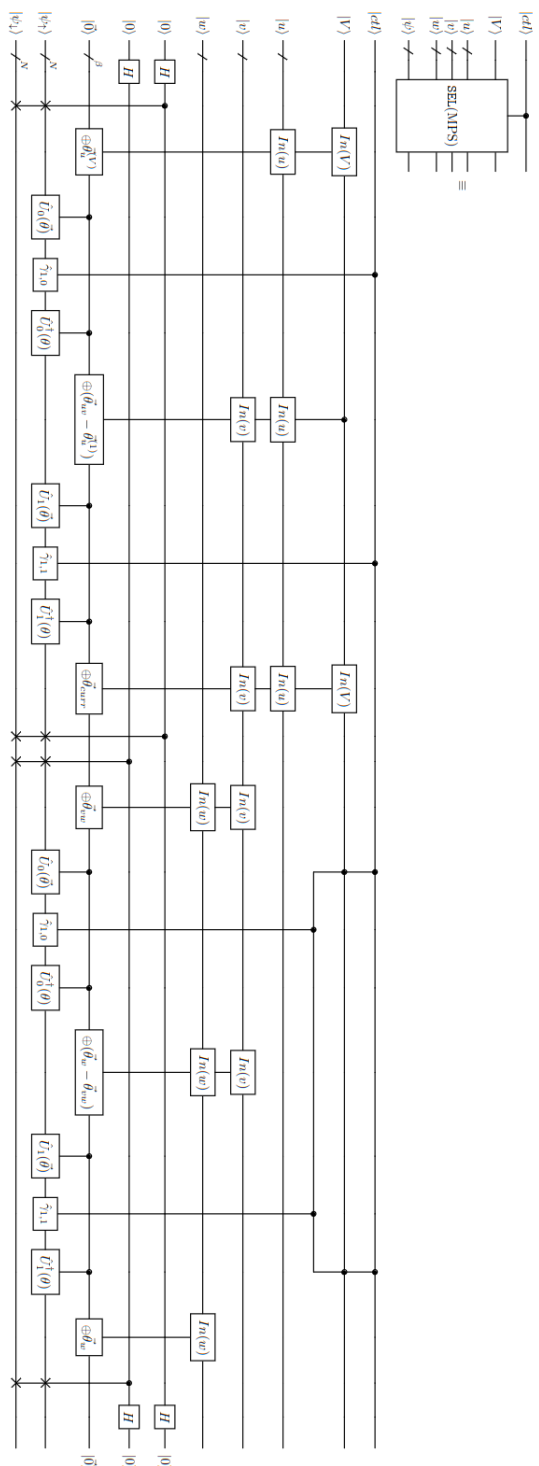


Figure 15. SELECT circuit for implementing L^4 -MPS LCU.

[1] D. S. Abrams and S. Lloyd, *Phys. Rev. Lett.* **83**, 5162 (1999).

[2] R. D. Somma, *New J. Phys.* **21** (2019).

[3] Y. Ge, J. Tura, and J. I. Cirac, *J. Math. Phys.* **60**, 022202 (2019).

[4] A. Aspuru-Guzik, A. D. Dutoi, P. J. Love, and M. Head-Gordon, *Science* **309**, 1704 (2005).

[5] L. Lin and Y. Tong, *PRX Quantum* **3** (2022).

[6] A. J. Moore, Y. Wang, Z. Hu, S. Kais, and A. M. Weiner, *New J. Phys.* **23**, 113027 (2021).

[7] A. Y. Kitaev, arXiv (1995), 10.48550/arxiv.quant-ph/9511026.

[8] D. W. Berry, C. Gidney, M. Motta, J. R. McClean, and R. Babbush, *Quantum* **3**, 208 (2019).

[9] G. Wang, D. Stilck-França, R. Zhang, S. Zhu, and P. D. Johnson, “Quantum algorithm for ground state energy estimation using circuit depth with exponentially improved dependence on precision,” (2022).

[10] S. Lloyd, *Science* **273**, 1073 (1996).

[11] M. Suzuki, *J. Math. Phys.* **32**, 400 (1991).

[12] K. Hejazi, M. S. Zini, and J. M. Arrazola, “Better bounds for low-energy product formulas,” (2024), arXiv:2402.10362 [quant-ph].

[13] M. Suzuki, *J. Math. Phys.* **32**, 400 (1991).

[14] A. M. Childs, Y. Su, M. C. Tran, N. Wiebe, and S. Zhu, *Phys. Rev. X* **11**, 011020 (2021).

[15] D. Poulin, M. B. Hastings, D. Wecker, N. Wiebe, A. C. Doberty, and M. Troyer, *Quantum Info. Comput.* **15**, 361–384 (2015).

[16] A. Gilyén, Y. Su, G. H. Low, and N. Wiebe, in *Proc. 51st ACM SIGACT Theor. Comput.* (2019) pp. 193–204.

[17] G. H. Low and I. L. Chuang, *Quantum* **3**, 163 (2019).

[18] D. Motlagh and N. Wiebe, “Generalized quantum signal processing,” (2023), arXiv:2308.01501 [quant-ph].

[19] A. M. Childs, R. Cleve, E. Deotto, E. Farhi, S. Gutmann, and D. A. Spielman, in *Proc. 35th ACM Symp. Theor. Comput.* (2003).

[20] J. Lee, D. W. Berry, C. Gidney, W. J. Huggins, J. R. McClean, N. Wiebe, and R. Babbush, *PRX Quantum* **2**, 3 (2021).

[21] A. M. Childs and N. Wiebe, *Quantum Info. Comput.* **12**, 901–924 (2012).

[22] G. H. Low and N. Wiebe, “Hamiltonian simulation in the interaction picture,” (2019), arXiv:1805.00675 [quant-ph].

[23] I. Loaiza, A. M. Khah, N. Wiebe, and A. F. Izmaylov, “Reducing molecular electronic hamiltonian simulation cost for linear combination of unitaries approaches,” (2022).

[24] V. von Burg, G. H. Low, T. Haner, D. Steiger, M. Reiher, M. Roetteler, and M. Troyer, *Phys. Rev. Research* **3**, 033055 (2021).

[25] I. Loaiza and A. F. Izmaylov, *J. Chem. Theory Comput.* **19**, 8201 (2023).

[26] O. Christiansen, *J. Chem. Phys.* **120** (2004).

[27] V. V. Shende and I. L. Markov, *Quantum Info. Comput.* **9**, 461–486 (2009).

[28] V. Shende, S. Bullock, and I. Markov, *IEEE Transactions on CAD* **25**, 1000 (2006).

[29] R. Babbush, C. Gidney, D. W. Berry, N. Wiebe, J. McClean, A. Paler, A. Fowler, and H. Neven, *Phys. Rev. X* **8** (2018).

[30] A. M. Childs, D. Maslov, Y. Nam, N. J. Ross, and Y. Su, *Proc. Natl. Acad. Sci.* **115**, 9456 (2018).

[31] E. Koridon, S. Yalouz, B. Senjean, F. Buda, T. E. O’Brien, and L. Visscher, *Phys. Rev. Research* **3**, 033127 (2021).

[32] G. K.-L. Chan, A. Keselman, N. Nakatani, Z. Li, and S. R. White, *J. Chem. Phys.* **145** (2016).

[33] T. G. Kolda and B. W. Bader, *SIAM Rev.* **51**, 455 (2009).

[34] H. A. L. Kiers, *J. Chemometrics* **14**, 105 (2000).

[35] R. A. Harshman, in *UCLA Working Papers in Phonetics*, 16 (1972).

[36] J. D. Carroll and J.-J. Chang, *Psychometrika* **35**, 283 (1970).

[37] F. L. Hitchcock, *J. Math. Phys.* **7**, 164 (1927).

[38] J. Mocks, *IEEE Trans. Biomed. Eng.* **35**, 482 (1988).

[39] E. Wigner and P. Jordan, *Z. Phys* **47**, 631 (1928).

[40] S. B. Bravyi and A. Y. Kitaev, *Ann. Phys.* **298**, 210 (2002).

[41] J. T. Seeley, M. J. Richard, and P. J. Love, *J. Chem. Phys.* **137**, 224109 (2012).

[42] A. Tranter, S. Sofia, J. Seeley, M. Kaicher, J. McClean, R. Babbush, P. V. Coveney, F. Mintert, F. Wilhelm, and P. J. Love, *Int. J. Quantum Chem.* **115**, 1431 (2015).

[43] A. F. Izmaylov, T.-C. Yen, R. A. Lang, and V. Verteletskyi, *J. Chem. Theor. Comput.* **16**, 190 (2020).

[44] J. M. Foster and S. F. Boys, *Rev. Mod. Phys.* **32**, 300 (1960).

[45] M. Motta, E. Ye, J. R. McClean, Z. Li, A. J. Minnich, R. Babbush, and G. K.-L. Chan, *npj Quantum Info.* **7** (2021).

[46] B. Peng and K. Kowalski, *J. Chem. Theor. Comput.* **13**, 4179 (2017).

[47] M. Motta, E. Ye, J. R. McClean, Z. Li, A. J. Minnich, R. Babbush, and G. K.-L. Chan, *npj Quantum Info.* **7** (2021).

[48] M. Motta, J. Shee, S. Zhang, and G. K.-L. Chan, *J. Chem. Theor. Comput.* **15**, 3510 (2019).

[49] Y. Matsuzawa and Y. Kurashige, *J. Chem. Theor. Comput.* **16**, 944 (2020).

[50] W. J. Huggins, J. R. McClean, N. C. Rubin, Z. Jiang, N. Wiebe, K. B. Whaley, and R. Babbush, *npj Quantum Info.* **7** (2021).

[51] D. W. Berry, C. Gidney, M. Motta, J. McClean, and R. Babbush, *Quantum* **3**, 208 (2019).

[52] T.-C. Yen and A. F. Izmaylov, *PRX Quantum* **2**, 4 (2021).

[53] O. Oumarou, M. Scheurer, R. M. Parrish, E. G. Hohenstein, and C. Gogolin, “Accelerating quantum computations of chemistry through regularized compressed double factorization,” (2022), arXiv:2212.07957 [quant-ph].

[54] J. Cohn, M. Motta, and R. M. Parrish, *PRX Quantum* **2** (2021).

[55] J. Lee, L. Lin, and M. Head-Gordon, *J. Chem. Theor. Comput.* **16**, 243 (2019).

[56] B. C. Hall, in *Lie Groups, Lie Algebras, and Representations: An Elementary Introduction* (Springer, Switzerland, 2015) p. 314.

[57] A. Szabo and N. Ostlund, *Modern Quantum Chemistry: Introduction to Advanced Electronic Structure Theory*, Dover Books on Chemistry (Dover Publications, 1996).

[58] K. Pierce and E. F. Valeev, “Efficient construction of canonical polyadic approximations of tensor networks,” (2022), arXiv:2208.09992 [physics.chem-ph].

[59] C. Jones, *Phys. Rev. A* **87** (2013).

[60] J. R. McClean, R. Babbush, P. J. Love, and A. Aspuru-Guzik, *J. Phys. Chem. Lett.* **5**, 4368 (2014).

[61] G. H. Low, V. Kliuchnikov, and L. Schaeffer, “Trading t-gates for dirty qubits in state preparation and unitary synthesis,” (2018), arXiv:1812.00954 [quant-ph].

[62] V. Gheorghiu, M. Mosca, and P. Mukhopadhyay, *npj Quantum Information* **8** (2022), 10.1038/s41534-022-00651-y.

[63] Y. R. Sanders, D. W. Berry, P. C. Costa, L. W. Tessler, N. Wiebe, C. Gidney, H. Neven, and R. Babbush, *PRX Quantum* **1**, 020312 (2020).

[64] M. B. Mansky, V. R. Puigvert, S. L. Castillo, and C. Linnhoff-Popien, “Decomposition algorithm of an arbitrary pauli exponential through a quantum circuit,” (2023), arXiv:2305.04807 [quant-ph].

[65] Q. Sun, *J. Comput. Chem.* **36**, 1664 (2015).

[66] Q. Sun, T. C. Berkelbach, N. S. Blunt, G. H. Booth, S. Guo, Z. Li, J. Liu, J. D. McClain, E. R. Sayfutyarova, S. Sharma, S. Wouters, and G. K.-L. Chan, *WIREs Comput. Mol. Sci.* **8**, e1340 (2018).

[67] Q. Sun, X. Zhang, S. Banerjee, P. Bao, M. Barbry, N. S. Blunt, N. A. Bogdanov, G. H. Booth, J. Chen, Z.-H. Cui, J. J. Eriksen, Y. Gao, S. Guo, J. Hermann, M. R. Hermes, K. Koh, P. Koval, S. Lehtola, Z. Li, J. Liu, N. Mardirossian, J. D. McClain, M. Motta, B. Mussard, H. Q. Pham, A. Pulkin, W. Purwanto, P. J. Robinson, E. Ronca, E. R. Sayfutyarova, M. Scheurer, H. F. Schurkus, J. E. T. Smith, C. Sun, S.-N. Sun, S. Upadhyay, L. K. Wagner, X. Wang, A. White, J. D. Whitfield, M. J. Williamson, S. Wouters, J. Yang, J. M. Yu, T. Zhu, T. C. Berkelbach, S. Sharma, A. Y. Sokolov, and G. K.-L. Chan, *J. Chem. Phys.* **153**, 024109 (2020).